Human cytomegalovirus protein pUL36: a dual cell death pathway inhibitor

Alice Fletcher-Etherington[a], Luis Nobre[a], Katie Nightingale[a], Robin Antrobus[a], Jenna Nichols[b], Andrew J. Davison[b], Richard J. Stanton[c], Michael P. Weekes[a,1]

Affiliations:
[a] Cambridge Institute for Medical Research, University of Cambridge, Hills Road, Cambridge CB2 0XY, UK
[b] MRC-University of Glasgow Centre for Virus Research, Sir Michael Stoker Building, 464 Bearsden Road, Glasgow G61 1QH, UK
[c] Cardiff University School of Medicine, Division of Infection and Immunity, Henry Wellcome Building, Heath Park, Cardiff CF14 4XN, UK
[1] Corresponding author

Correspondence:
Michael P. Weekes
Email: mpw1001@cam.ac.uk

ORCIDs
Alice Fletcher-Etherington: 0000-0001-7313-9247
Andrew J. Davison: 0000-0002-4991-9128
Richard J. Stanton: 0000-0002-6799-1182
Michael P. Weekes: 0000-0003-3196-5545

Classification:
Major category: Biological Sciences
Minor category: Microbiology

Key words: human cytomegalovirus; cell death; necroptosis; protein degradation; MLKL

Author contributions:
AFE designed research, performed research, analyzed data and wrote the paper.
LN performed research and edited the paper
KN performed research and edited the paper
RA performed research
JN performed research
AJD contributed new reagents/analytic tools, analyzed data and edited the paper
RJS contributed new reagents/analytic tools and edited the paper
MPW designed research, analyzed data and wrote the paper

Competing interest statement: The authors declare no competing interests.

This file includes:
Abstract and Significance Statement
Main text (Introduction, Results, Discussion, Materials and Methods, Acknowledgements and References)
Figure legends for Figures 1-5 (Figures have been uploaded as separate PDF files)

ABSTRACT

Human cytomegalovirus (HCMV) is an important human pathogen and a paradigm of intrinsic, innate and adaptive viral immune evasion. Here, we employed multiplexed tandem mass tag-based proteomics to characterise host proteins targeted for degradation late during HCMV infection. This approach revealed that mixed lineage kinase domain-like protein (MLKL), a key terminal mediator of cellular necroptosis, was rapidly and persistently degraded by the minimally passaged HCMV strain Merlin but not the extensively passaged strain AD169. The strain Merlin viral inhibitor of apoptosis pUL36 was necessary and sufficient both to degrade MLKL and to inhibit necroptosis. Furthermore, mutation of pUL36 Cys^{131} abrogated MLKL degradation and restored necroptosis. As the same residue is also required for pUL36-mediated inhibition of apoptosis by preventing proteolytic activation of procaspase-8, we define pUL36 as a multifunctional inhibitor of both apoptotic and necroptotic cell death.

SIGNIFICANCE STATEMENT

Cell death is a key defence against viral infection, preventing spread from infected to uninfected cells. Correspondingly, certain viruses encode inhibitors of apoptotic and necroptotic cell death pathways in order to facilitate their persistence. Human cytomegalovirus (HCMV) is an important human pathogen that can block apoptosis, but hitherto it has been unclear whether or how the virus blocks necroptosis. Here, we used a proteomic screen to identify human proteins targeted for destruction by HCMV, finding that the key necroptosis mediator MLKL is degraded throughout infection. MLKL is targeted for degradation by HCMV protein pUL36, which is also instrumental in inhibiting apoptosis. Thus, pUL36 is a dual cell death pathway inhibitor, and may represent an important therapeutic target.

INTRODUCTION

Human cytomegalovirus (HCMV) infects the majority of the world's population, with a seroprevalence of 60-80% in Western Europe and the USA, and up to 100% in developing countries (1, 2). Following primary infection, a latent infection is established that persists lifelong. Reactivation from latency to productive infection in immunocompromised people can lead to significant morbidity or mortality, in addition to allograft rejection in transplant recipients (3, 4). Furthermore, HCMV is the commonest infectious cause of congenital disease, affecting ~1/200 pregnancies (5).

Only four drugs are approved by the FDA to treat HCMV, and all are associated with significant toxicity and the threat of drug resistance (2, 6). Small molecule-based disruption of interactions between antiviral host proteins and their viral antagonists could facilitate endogenous inhibition of viral replication (7, 8). Identification and detailed characterisation of such interactions thus has important implications for the development of novel anti-HCMV therapies.

HCMV encodes 170 canonical protein-coding genes (2). A substantial number of additional, non-canonical open reading frames (ORFs) that potentially encode proteins have been identified by ribosomal footprinting and proteomics (9, 10). During productive infection in vitro, expression of HCMV genes is conventionally divided into immediate-early, early and late phases during a ~96 h lytic replication cycle. Recently, five temporal classes of viral protein expression (Tp1-Tp5) have been defined by measuring viral protein profiles over the whole course of infection (11).

Hijacking of the ubiquitin-proteasome system (UPS) to degrade host proteins is ubiquitous across many viral families (12). The proteins degraded by viruses are typically detrimental to viral replication, and can include antiviral restriction factors or components of viral sensing pathways, activating immune cell ligands, and elements of cell death pathways (13, 14). We have shown previously that >900 host proteins are downregulated >3-fold over the course of HCMV infection, with 133 proteins degraded during the early phase, of which 89% are targeted to the proteasome. These data led directly to the identification of candidate natural killer (NK) cell ligands and identified helicase-like transcription factor (HLTF) as a novel antiviral restriction factor (10, 11). However, it is not yet known which proteins are degraded later during infection, or throughout a whole infection time-course. Furthermore, it is unclear whether or how HCMV inhibits necroptotic cell death pathways, which represent a key defence against viral spread within an infected host (15).

Activation of death receptors such as TRAILR1/2, TNFR1 and Fas leads to apoptotic cell death via an activating cleavage of procaspase-8 (16). In the presence of caspase inhibition or limiting levels of ATP, extrinsic apoptosis shifts towards the necroptotic pathway. This is dependent on an interaction between Receptor Interacting Serine/Threonine Kinases 1 and 3 (RIP1/3) through their homotypic interaction motif (RHIM) domains (17). Necroptosis can also be activated by cytoplasmic sensing of murine

cytomegalovirus (MCMV) DNA by Z-DNA-binding protein 1 (ZBP1), or ligation of Toll-like receptors 3 or 4 (TLR3/4), which activate RIP3 through alternative RHIM domain-containing adaptors (17) **(Figure 1)**. All three pathways converge with RIP3-dependent phosphorylation and activation of the pseudokinase MLKL, which transitions from an inactive monomer to a necroptotic oligomer. The oligomer translocates to and disrupts the plasma membrane, leading to cell swelling and loss of plasma membrane integrity, although the exact mechanism of membrane disruption is unclear (18–20).

Here, a systematic examination of protein degradation at 48 h of HCMV infection determined that degradation of MLKL was sustained throughout early and late infection. The data showed that MLKL was degraded by the minimally-passaged Merlin strain of HCMV, but not by the highly passaged laboratory-adapted strain AD169. The strain Merlin UL36-encoded viral inhibitor of caspase-8 activation (vICA/pUL36), which is known to function as a potent inhibitor of apoptosis, interacted with MLKL and was necessary and sufficient both to degrade MLKL and to inhibit TNFα-stimulated necroptosis. Whereas HCMV strain AD169 sensitised cells to necroptosis, strain Merlin prevented this sensitisation. pUL36 is thus a multifunctional cell death inhibitor capable of inhibiting both apoptotic and necroptotic pathways.

RESULTS

Host proteins targeted for degradation at 48 h of HCMV infection

We applied the proteasomal inhibitor MG132 to build a global picture of proteins degraded late during HCMV infection. TERT-immortalised primary human fetal foreskin fibroblasts (HFFF-TERTs) were infected with HCMV strain Merlin at a multiplicity of infection (MOI) of 10 for 48 h, with application of MG132 (or the equivalent amount of DMSO as a control) for the final 12 h of infection **(Figure 2A)**. MG132 is known to inhibit calpains and lysosomal cathepsins in addition to the proteasome (10), and was used to generate a comprehensive list of proteins targeted for degradation by HCMV rather than to identify proteins specifically degraded by the proteasome. 8,476 human and 186 viral proteins were quantified across two biological replicates (**Dataset S1**, which includes an interactive 'Plotter'). Two ratios and associated significance values were calculated for each protein: (i) virus:mock infection and (ii) virus+MG132:virus infection **(Figure 2B)**. 52 proteins met high confidence criteria for degradation, with a fold downregulation and rescue of >2 and $p<0.05$ for both ratios.

From a comparison with our previous study of HCMV-induced protein degradation between 2-24 h (10), seven proteins were degraded with high confidence throughout early and late infection **(Figures 2C, 2D)**. These proteins included HLTF and Anaphase Promoting Complex subunits 1 and 5 (ANAPC1/5), whose degradation by HCMV has been well characterised (10, 21). The effector of necroptosis MLKL was the most significantly downregulated protein at 48 h of HCMV infection and was among proteins most significantly rescued by addition of MG132 **(Figure 2B)**. In comparison, 37

proteins degraded at 48 h did not score highly for degradation at early time points (10) **(Figures 2C, 2E, and SI Appendix, Figure S1A)**.

Degradation of MLKL is mediated by immediate early protein pUL36

We previously took a systematic approach to identifying the viral proteins responsible for the degradation of host factors, employing a panel of recombinant viruses deleted for various blocks of HCMV genes that are non-essential for replication *in vitro* (10). These viruses included strain AD169, a highly passaged, laboratory-adapted strain that contains a deletion in the U_L/b' region (encoding 20 canonical genes, UL133-UL150A), frameshifts in RL5A, RL13 and UL131A, and a non-synonymous substitution in UL36 that inactivates the ability of pUL36 to bind procaspase-8 and inhibit apoptosis (22, 23). MLKL was downregulated by strain Merlin viruses but not by strain AD169, and this was confirmed by immunoblotting **(Figures 3A-B)**. This indicated that one or more differences in AD169 abrogate virus-mediated MLKL degradation. To identify viral factors interacting with MLKL, a SILAC immunoprecipitation (IP) was performed in HCMV strain Merlin-infected HFFF-TERTs stably expressing MLKL tagged with HA at the C-terminus. pUL36 co-precipitated with MLKL, and this was confirmed by a reciprocal IP **(Figures 3C-D, Dataset S2)**. This interaction was further supported by an immunofluorescence study showing cytoplasmic co-localisation between MLKL-HA and pUL36 in stably expressing HFFF-TERTs **(SI Appendix, Figure S2A)**. To determine whether pUL36 interacts with inactive, unphosphorylated MLKL or active, phosphorylated MLKL we re-searched the pUL36-V5 SILAC IP data (**Figure 3D**) using a variable phospho-modification. All identified MLKL peptides were unphosphorylated, and encompassed all known sites of activating phospho-modifications **(SI Appendix, Figure S3)**. This suggests that pUL36 interacts with unphosphorylated MLKL but does not exclude an additional interaction with phosphorylated MLKL.

A series of HFFF-TERT cell lines stably expressing strain Merlin UL36 or each of the individual genes in the UL133-UL150A region were next screened to determine whether any other viral protein contributed to MLKL degradation. Expression of UL36 was sufficient to reduce the level of MLKL by 3.7-fold **(Figure 3E and SI Appendix, Figures S2B-D)**. MLKL expression was not modulated more than 2-fold by any other proteins in the U_L/b' region. Despite substantial variation in the level of expression of some of the viral proteins, this did not correlate with relative MLKL abundance **(SI Appendix, Figure S2D)**. pUL36 could be detected from 6 hpi, and was expressed with Tp2 (temporal protein profile 2) kinetics, matching the kinetics of MLKL degradation (11) **(Figure 3F)**. Finally, infection with strain AD169 or two independent strain Merlin UL36 deletion mutants rescued MLKL, suggesting that pUL36 was necessary as well as sufficient for MLKL degradation **(Figure 3G)**.

pUL36 protects cells from necroptosis

Inhibition of caspase-8 during death receptor stimulation shifts extrinsic apoptosis towards the necroptotic pathway (24–26). The HCMV UL36-encoded viral inhibitor of caspase-8 activation (vICA/pUL36) inhibits apoptosis by binding the pro-domain of caspase-8 and preventing its proteolytic activation (23). Inhibition of caspase-8 activation by pUL36 would be predicted to promote necroptosis, but this has not been reported. We therefore sought to determine whether Merlin pUL36 additionally inhibits necroptosis by degrading MLKL. *In vitro*, necroptosis can be stimulated by a combination of TNFα (T), BV6 (B, an IAP antagonist that sensitises cells to TNFα-induced cell death), and the pan-caspase inhibitor Z-VAD-fmk (Z) **(Figure 4A)** (27, 28). Although previous reports have suggested that HFFFs are not susceptible to necroptosis due to limiting levels of RIP3 (29), both RIP3 and RIP1 were detectable in HFFF-TERTs by proteomics **(SI Appendix, Figure S4A)**. Necroptosis was induced by T+B+Z (TBZ) in HFFF-TERTs as well as in immortalised mouse embryonic fibroblasts (MEFs), which are highly susceptible to necroptosis (30) and were therefore used as a positive control **(Figure 4B)**. Two inhibitors were employed to determine whether the stimulated death pathway was canonical MLKL- and RIP3-dependent necroptosis **(Figure 1)**. GSK'872 binds to and inhibits the RIP3 kinase domain (31, 32), whereas necrosulfonamide (NSA) inhibits downstream effector functions of MLKL via covalent reaction with the Cys^{86} residue of human but *not* murine MLKL (19, 33). NSA and GSK'872 inhibited TBZ-induced cytotoxicity in HFFF-TERTs, indicating that these cells expressed sufficient RIP3 to induce measurable canonical necroptosis **(Figure 4B)**.

Omoto *et al*. previously demonstrated that pUL36 does not impact the ability of HCMV strain Towne to protect against necroptosis in fibroblasts stably transduced with RIP3 (29). In contrast to this conclusion, we found that strain Merlin pUL36 was sufficient to inhibit necroptosis **(Figure 4C)**. The two other HCMV-encoded inhibitors of apoptosis, pUL37x1/vMIA (viral mitochondria-localized inhibitor of apoptosis) and pUL38 (34, 35), augmented MLKL-dependent necroptosis (as demonstrated by complete inhibition by NSA). However, cell death was incompletely inhibited by GSK'872, suggesting that a RIP3-independent mechanism might be acting in addition **(Figure 4C)**. Next, untransduced, control and UL36-expressing cell lines were treated with TB or TBZ in parallel to assess the effect of pUL36 on apoptosis and necroptosis respectively **(Figure 4D)**. Other inhibitors of caspase-8, including MCMV pM36 and the compound z-VAD-fmk (Z), inhibit death receptor-stimulated apoptosis while sensitising cells expressing sufficient levels of RIP3 and MLKL to necroptosis (24–26). Consistent with these observations, we detected no change in the overall level of cell death in untransduced cells when Z was added to TB **(Figure 4D left panel leftmost bar and right panel leftmost bar)**. In contrast, pUL36 was able to inhibit apoptotic cell death stimulated by TB, suggesting that it was not simply acting as a caspase-8 inhibitor **(Figure 4D left panel)**. Furthermore, in the presence of TBZ apoptosis is potently inhibited by the addition of Z, and pUL36 inhibited necroptotic

cell death **(Figure 4D right panel)**. Together these data indicate that pUL36 can inhibit both apoptosis and necroptosis.

Finally, infection of HFFFs with HCMV strains Merlin and AD169 for 48 h prior to TBZ stimulation suggested that inhibition of MLKL-dependent necroptosis required functional pUL36. Pre-infection with Merlin had a slight protective effect on necroptosis, whereas AD169 infection amplified the effect of TBZ **(Figures 4E-F)**. Cell death induced by TBZ after infection with HCMV also appeared to have a RIP3-independent component, as GSK'872 had little inhibitory effect.

Substitution of Merlin pUL36 Cys^{131} abrogates inhibition of necroptosis by abolishing MLKL binding and degradation

Strain Merlin and strain AD169 pUL36 differ by five amino acid residues **(SI Appendix, Figure S5)**, including a Merlin Cys^{131} → AD169 Arg^{131} substitution. This single replacement abrogates inhibition of apoptosis, as pUL36 can no longer bind procaspase-8 (23). Five Merlin pUL36 mutants corresponding to the five amino acid substitutions between strain Merlin and strain AD169 were constructed in order to determine which were important for degradation of MLKL. Only the C131R substitution prevented pUL36 from binding and downregulating MLKL (**Figure 5A-B**). The same pUL36 mutant was also unable to protect cells from necroptosis, suggesting that this single residue plays a key functional role in inhibition of both apoptosis and necroptosis by pUL36 **(Figure 5C)**.

DISCUSSION

Herpesviruses persist lifelong in infected individuals by comprehensive modulation of adaptive and innate immunity. Multiple viral proteins are deployed to target host factors for degradation, many very early during infection (10). The present study provides a systematic, searchable database that examines host protein degradation at 48 h of HCMV strain Merlin infection, approximately 50-66% of the way through the lytic replication cycle in HFFFs. In addition to identifying proteins degraded throughout the HCMV replication cycle, these data may be particularly useful for identifying which viral protein targets a given host factor for degradation. We defined previously the kinetics of expression of the majority of canonical HCMV proteins, which can now be compared to the kinetics of host protein degradation, from 6 to 48 h post-infection (10, 11). Other mechanisms of host protein degradation that are not inhibited by MG132 are also likely to be subverted by HCMV. However, 87-89% of degraded proteins were targeted to the proteasome by 24 h post-infection (10).

The key roles of necroptosis in protecting cell populations against virus infection are highlighted by the impressive range of known viral countermeasures. Necroptosis inhibitors are particularly widespread amongst herpesviruses, with MCMV and herpes simplex viruses (HSV) types 1 and 2 encoding conserved RHIM-domain containing proteins (M45, ICP6 and ICP10, respectively) which compete

with host RHIM-domain adaptor proteins such as RIP1 for binding to RIP3 (36–38). The HCMV M45 ortholog pUL45 does not contain a RHIM-domain and does not inhibit cell death (39). Instead, it had been suggested that HCMV targets the necroptotic pathway downstream of RHIM signalling, after RIP3-dependent phosphorylation of MLKL, although the mechanism had not been elucidated (29).

As other viral inhibitors of caspase-8 activation have been shown to sensitise cells to programmed necrosis (26, 40), it has been assumed that HCMV pUL36 would have a similar effect, requiring HCMV to encode a separate mechanism of necroptosis inhibition in order to evade cell death completely. However, although MCMV M36 can sensitise cells to necroptosis (26), the same phenomenon has not been demonstrated for HCMV pUL36, which may not be surprising given that both proteins exhibit only 19% sequence identity (41). The understanding of why HCMV pUL36 expression can inhibit death receptor-stimulated apoptosis instead of stimulating necroptosis as per the action of other inhibitors of caspase-8 such as z-VAD-fmk and MCMV M36 (24–26) may have been confounded by the use of cell lines that are not susceptible to necroptotic cell death (23). Here, we explain these observations by showing that HCMV pUL36 mediates the degradation of MLKL and inhibits necroptosis. In the presence of either UL36 expression or HCMV Merlin infection, the level of MLKL protein was decreased in cells lysed in either 6M guanidine, RIPA or 2% SDS, and subsequently rescued by the addition of MG132. Future work should confirm that high molarity guanidine and high percentage SDS do indeed fully solubilise RIPA-insoluble MLKL complexes that arise in cells undergoing necroptosis.

Previous studies investigating the interaction between HCMV and necroptosis have employed HFFFs stably transduced with RIP3 in order to confer susceptibility to necroptosis, which can otherwise be lost during cell propagation (29). Using these cells, the authors found that all tested HCMV strains, including AD169, were able to inhibit TNFα-stimulated necroptosis, although strain Merlin inhibited necroptosis more potently than AD169, consistent with our results **(Figure 4E)**. Furthermore, comparison of a WT strain Towne (encoding pUL36 with a cysteine at position 131) with a Towne ΔUL36 mutant suggested that pUL36 was necessary for inhibition of apoptosis but *not* necroptosis (29). In addition to mediating cell death, RIP3 has been implicated in NF-kB and inflammasome activation and can induce apoptosis when overexpressed (32, 42). It is possible that overexpression of RIP3 has off-target effects, which may explain the discrepancy between the previously published work and the present study; the experimental setting may clearly influence the outcome observed with pUL36. In addition, while the Omoto *et al*. study suggested that HCMV targets necroptosis downstream of MLKL phosphorylation, all MLKL peptides in our pUL36-V5 SILAC IP were unphosphorylated **(Figure 3D and SI Appendix, Figure S3)**, suggesting that pUL36 affects the monomeric MLKL pool. However, this does not exclude the potential for additional HCMV-mediated direct or indirect mechanisms of necroptosis inhibition. Further evidence that results can be dependent on cell type and the presence of RIP3 overexpression came from use of the Towne ΔUL36 mutant to show that pUL36 can inhibit caspase-independent cell death during late stages of macrophage differentiation (43). This also suggests

that pUL36-mediated degradation of MLKL may occur in more than one cell type. The HFFF-TERT cell line used in the present study is susceptible to RIP3 and MLKL-dependent canonical necroptosis **(Figure 4B)** and may be an invaluable resource for future studies of viral modulation of cell death.

Necroptotic activation of MLKL can influence many other cellular processes, including inflammasome activation, endosomal trafficking, extracellular vesicle generation and autophagy (44–47). It is therefore possible that HCMV-mediated degradation of MLKL may have other consequences for viral pathogenesis, including effects on virion assembly, trafficking and cell-to-cell spread.

Infection of HFFF-TERTs with HCMV prior to TBZ stimulation resulted in induction of a form of cell death that was not completely inhibited by GSK'872, which is suggestive of an RIP3-independent but MLKL-dependent mechanism **(Figure 4E)**. A similar but less significant effect was observed in cells expressing the HCMV apoptosis inhibitors pUL37 and pUL38 **(Figure 4C)**. RIP3-independent necroptosis in fibroblasts has been reported previously by others (30) but remains poorly characterised. Infection with HCMV strain AD169, which lacks a functional pUL36 protein, sensitised cells to necroptosis **(Figure 4E)**, in accord with the observed increase in MLKL protein upon infection with viruses deficient in functional pUL36 **(Figure 3G)**. This is likely to be due to IFN-mediated upregulation of MLKL (48). Strain Merlin protein pUL36 was able to counteract the effect of necroptosis sensitisation, rather than abrogating necroptosis entirely **(Figure 4E)**.

pUL36 can bind both pro-caspase-8 (23) and MLKL, facilitating potent inhibition of both apoptosis and necroptosis. Indeed, these two functions can be inhibited by the same single amino acid substitution gained during passage of HCMV in cell culture (22, 23). This suggests that a larger cell death complex may form from the caspase-8:FADD:RIP1 FADDosome/Ripoptosome (49–51) and the RIP1:RIP3 necrosome (17), enabling an interaction between pUL36, caspase-8 and MLKL. Examination of this hypothesis, including an investigation of whether binding of pUL36 to caspase-8 is a necessary intermediary for binding to MLKL, would be of significant interest to the field.

HCMV pUL36 and its orthologs belong to the US22 family of herpesvirus proteins, which characteristically feature a set of motifs I to IV (41). Cys^{131}, which is found within motif III, is conserved within the primate cytomegaloviruses but is replaced by conservative substitutions in rodent cytomegalovirus orthologs that do not abrogate apoptosis inhibition. In addition, the MCMV ortholog pM36, which displays only 19% sequence similarity to HCMV pUL36 and lacks the region that includes Cys^{131}, is still an efficient suppressor of apoptosis (41). This suggests that the Arg^{131} residue of strain AD169 pUL36 may restrict cell death inhibition, as opposed to Cys^{131} being required for this function.

Only four drugs are currently available for treating HCMV, all exhibiting significant adverse effects and the potential of drug resistance. The identification of a potentially inhibitable interaction between a single residue of a viral antagonist and key mediators of both necroptosis and apoptosis may therefore be of substantial therapeutic significance. In addition to pUL36-MLKL, other interactions involving

distinct antiviral pathways could be targeted simultaneously to potently inhibit viral replication, for example between HCMV pUL145 and the recently identified restriction factor HLTF (10). Moreover, our data are likely to identify further proteins that have roles in restricting infection by HCMV or other viruses.

MATERIALS AND METHODS

Extended materials and methods can be found in the SI Appendix.

Viral infections

The required volume of viral stock to achieve the multiplicity of infection (MOI) described in the results section was diluted in serum-free Dulbecco's modified Eagle's medium (DMEM), mixed gently and applied to HFFF-TERTs. Mock infections were performed identically but with DMEM instead of viral stock. Time zero was considered the time at which cells first came into contact with virus. Cells were incubated with virus for 2 h at 37 °C on a rocking platform, and then the medium was replaced with DMEM + 10% FBS.

Proteomic Screen

HFFFs-TERTs were infected as described above in biological duplicate at an MOI of 10. At 36 hpi, 10 μM MG132 or the equivalent volume of DMSO was added to the cells for the last 12 h of infection. Samples from the second replicate were digested and analysed with residual samples from the 12 h degradation screen from the Nightingale *el al.* study (10). Methods for whole cell lysate protein preparation and digestion, peptide labelling with tandem mass tags, HpRP fractionation, liquid chromatography-mass spectrometry and data analysis are discussed in detail in the Nightingale *et al.* study (10) and recapitulated in the SI.

Immunoblotting

Cells were lysed, sonicated and clarified by centrifugation, and protein concentration was measured using a bicinchoninic acid (BCA) assay. Samples were denatured and reduced, and then the proteins were separated by SDS polyacrylamide gel electrophoresis (PAGE), transferred to a polyvinylidene difluoride (PVDF) membrane (0.45 μm pore), and probed using the primary and secondary antibodies detailed in the SI. Fluorescent signals were detected using the Odyssey CLx Imaging System (LI-COR), and images were processed and quantified using Image Studio Lite V5.2 (LI-COR).

Plasmid construction and transduction

Lentiviral expression vectors encoding MLKL-HA, the V5-tagged viral proteins pUL36 and pUL133-pUL150A and controls, were synthesised by PCR amplification of the genes and cloning them into Gateway vectors (52). V5-tagged UL36 point mutants were generated by PCR site-directed

mutagenesis. The primers and templates used are described in the SI. Stable cell lines were generated by transduction with lentiviruses produced via the transfection of HEK293T cells with lentiviral expression vectors and helper plasmids.

Immunoprecipitation

Cells were harvested in lysis buffer, tumbled on a rotator and then clarified by centrifugation and filtration. After incubation with immobilised mouse monoclonal anti-V5 or anti-HA agarose resin, samples were washed and then subjected either to immunoblotting or mass spectrometry (see SI).

Cell death assays

For assays in the absence of infection, 96-well plates were seeded with HFFF-TERTs or immortalised MEFs and incubated for 24 h. Cells were incubated for 18 h with 30 ng/ml TNFα, 5 μM BV-6 and/or 25 μM z-VAD-fmk in the presence or absence of 0.5 μM necrosulfonamide (NSA) or 1.5 μM GSK'872, or DMSO alone (control). Half of the control cells were lysed to measure lactate dehydrogenase (LDH) release from maximally lysed cells. The other half were used to measure background LDH release from live, untreated cells. LDH release was measured using the CytoTox 96® Non-Radioactive Cytotoxicity Assay. Average absorbance values derived from culture medium alone were subtracted from each absorbance value from experimental wells. For assays in the presence of infection, HFFF-TERTs were seeded into 96-well plates, incubated for 24 h, and infected with HCMV (MOI = 5). The medium was changed 48 h after infection to stimulate necroptosis as described above.

Data and materials availability statement

The mass spectrometry proteomics data have been deposited to the ProteomeXchange Consortium (http://www.proteomexchange.org/) via the PRIDE partner repository (53) with the dataset identifier PXD017279. All materials described in this manuscript, and any further details of protocols employed, can be obtained on request from the corresponding author by email to mpw1001@cam.ac.uk.

ACKNOWLEDGEMENTS

We are grateful to Prof. Steve Gygi for providing access to the "MassPike" software pipeline for quantitative proteomics. This work was supported by an MRC studentship (MR/N013433/1) to AFE, a Wellcome Trust Senior Clinical Research Fellowship (108070/Z/15/Z) to MPW, an MRC Project Grant (MR/P001602/1) to RJS, and an MRC Programme Grant (MC_UU_12014/3) to AJD. This study was additionally supported by the Cambridge Biomedical Research Centre, UK.

REFERENCES

1. M. J. Cannon, D. S. Schmid, T. B. Hyde, Review of cytomegalovirus seroprevalence and demographic characteristics associated with infection. *Rev. Med. Virol.* **20**, 202–213 (2010).
2. E. S. Mocarski, T. Shenk, P. Griffiths, R. F. Pass, "Cytomegaloviruses" in *Fields Virology Sixth Edition*, (2013).
3. P. Reinke, S. Prösch, F. Kern, H. D. Volk, Mechanisms of human cytomegalovirus (HCMV) (re)activation and its impact on organ transplant patients. *Transpl. Infect. Dis.* **1**, 157–64 (1999).
4. W. G. Nichols, L. Corey, T. Gooley, C. Davis, M. Boeckh, High risk of death due to bacterial and fungal infection among cytomegalovirus (CMV)–seronegative recipients of stem cell transplants from seropositive donors: evidence for indirect effects of primary CMV infection. *J. Infect. Dis.* **185**, 273–282 (2002).
5. W. J. Britt, Congenital human cytomegalovirus infection and the enigma of maternal immunity. *J. Virol.* **91** (2017).
6. B. Hock Tan, Cytomegalovirus treatment. *Curr. Treat. Options Infect. Dis.* **6**, 256–270 (2014).
7. R. Nathans, *et al.*, Small-molecule inhibition of HIV-1 Vif. *Nat Biotechnol* **26**, 1187–1192 (2008).
8. S. Cen, *et al.*, Small molecular compounds inhibit HIV-1 replication through specifically stabilizing APOBEC3G. *J. Biol. Chem.* **285**, 16546–16552 (2010).
9. N. Stern-Ginossar, *et al.*, Decoding human cytomegalovirus. *Science (80-.).* **338** (2012).
10. K. Nightingale, *et al.*, High-definition analysis of host protein stability during human cytomegalovirus infection reveals antiviral factors and viral evasion mechanisms. *Cell Host Microbe* **24**, 1–14 (2018).
11. M. P. Weekes, *et al.*, Quantitative Temporal Viromics: an approach to investigate host-pathogen interaction. *Cell* **157**, 1460–1472 (2014).
12. A. Halenius, C. Gerke, H. Hengel, Classical and non-classical MHC I molecule manipulation by human cytomegalovirus: so many targets—but how many arrows in the quiver? *Cell. Mol. Immunol.* **12**, 139–153.
13. K. Viswanathan, K. Früh, V. DeFilippis, Viral hijacking of the host ubiquitin system to evade interferon responses. *Curr. Opin. Microbiol.* **13**, 517–523 (2010).
14. Q. Tang, P. Wu, H. Chen, G. Li, Pleiotropic roles of the ubiquitin-proteasome system during viral propagation. *Life Sci.* **207**, 350–354 (2018).
15. W. J. Kaiser, J. W. Upton, E. S. Mocarski, Viral modulation of programmed necrosis. *Curr. Opin. Virol.* **3**, 296–306 (2013).
16. R. C. Taylor, S. P. Cullen, S. J. Martin, Apoptosis: controlled demolition at the cellular level.

Nat. Rev. Mol. Cell Biol. **9**, 231–241 (2008).

17. J. Zhang, Y. Yang, W. He, L. Sun, Necrosome core machinery: MLKL. *Cell. Mol. Life Sci.* **73**, 2153–2163 (2016).
18. X. Chen, *et al.*, Translocation of mixed lineage kinase domain-like protein to plasma membrane leads to necrotic cell death. *Cell Res.* **24**, 105–121 (2014).
19. L. Sun, *et al.*, Mixed lineage kinase domain-like protein mediates necrosis signaling downstream of RIP3 kinase. *Cell* **148**, 213–227 (2012).
20. E. J. Petrie, P. E. Czabotar, J. M. Murphy, The structural basis of necroptotic cell death signaling. *Trends Biochem. Sci.* **44**, 53–63 (2019).
21. E. Clark, D. H. Spector, Studies on the contribution of human cytomegalovirus UL21a and UL97 to viral growth and inactivation of the Anaphase-Promoting Complex/Cyclosome (APC/C) E3 ubiquitin ligase reveal a unique cellular mechanism for downmodulation of the APC/C subunits APC1,. *J. Virol.* **89**, 6928–6939 (2015).
22. A. J. Bradley, *et al.*, High-throughput sequence analysis of variants of human cytomegalovirus strains Towne and AD169. *J. Gen. Virol.* **90**, 2375–80 (2009).
23. A. Skaletskaya, *et al.*, A cytomegalovirus-encoded inhibitor of apoptosis that suppresses caspase-8 activation. *PNAS* **98**, 7829–7834 (2001).
24. N. Holler, *et al.*, Fas triggers an alternative, caspase-8-independent cell death pathway using the kinase RIP as effector molecule. *Nat. Immunol.* **1**, 489–495 (2000).
25. S. McComb, *et al.*, Cathepsins limit macrophage necroptosis through cleavage of RIP1 kinase. *J. Immunol.* **192**, 5671–5678 (2014).
26. W. J. Kaiser, *et al.*, RIP3 mediates the embryonic lethality of caspase-8-deficient mice. *Nature* **471**, 368–373 (2011).
27. M. El-Mesery, M. E. Shaker, A. Elgaml, The SMAC mimetic BV6 induces cell death and sensitizes different cell lines to TNF-α and TRAIL-induced apoptosis. *Exp. Biol. Med. (Maywood).* **241**, 2015–2022 (2016).
28. N. M. De Vasconcelos, N. Van Opdenbosch, H. Van Gorp, E. Parthoens, M. Lamkanfi, Single-cell analysis of pyroptosis dynamics reveals conserved GSDMD-mediated subcellular events that precede plasma membrane rupture. *Cell Death Differ.* **26**, 146–161 (2019).
29. S. Omoto, *et al.*, Suppression of RIP3-dependent necroptosis by human cytomegalovirus. *J. Biol. Chem.* **290**, 11635–11648 (2015).
30. D.-W. Zhang, *et al.*, Multiple death pathways in TNF-treated fibroblasts: RIP3- and RIP1-dependent and independent routes. *Cell Res.* **21**, 368–371 (2011).
31. W. J. Kaiser, *et al.*, Toll-like receptor 3-mediated necrosis via TRIF, RIP3, and MLKL. *J. Biol. Chem.* **288**, 31268–79 (2013).
32. P. Mandal, *et al.*, RIP3 induces apoptosis independent of pro-necrotic kinase activity. *Mol Cell* **56**, 481–495 (2014).

33. S. Liu, *et al.*, MLKL forms disulfide bond-dependent amyloid-like polymers to induce necroptosis. *Proc. Natl. Acad. Sci. U. S. A.* **114**, E7450–E7459 (2017).
34. C. E. Andoniou, M. A. Degli-Esposti, Insights into the mechanisms of CMV-mediated interference with cellular apoptosis. *Immunol. Cell Biol.* **84**, 99–106 (2006).
35. S. Terhune, *et al.*, Human cytomegalovirus UL38 protein blocks apoptosis. *J. Virol.* **81**, 3109–23 (2007).
36. H. Guo, W. J. Kaiser, E. S. Mocarski, Manipulation of apoptosis and necroptosis signaling by herpesviruses. *Med Microbiol Immunol* **204**, 439–448 (2015).
37. J. W. Upton, W. J. Kaiser, E. S. Mocarski, DAI/ZBP1/DLM-1 complexes with RIP3 to mediate virus-induced programmed necrosis that is targeted by murine cytomegalovirus vIRA. *Cell Host Microbe* **11**, 290–297 (2012).
38. H. Guo, *et al.*, Herpes simplex virus suppresses necroptosis in human cells. *Cell Host Microbe* **17**, 243–251 (2015).
39. M. Patrone, *et al.*, The human cytomegalovirus UL45 gene product is a late, virion-associated protein and influences virus growth at low multiplicities of infection. *J. Gen. Virol.* **84**, 3359–3370 (2003).
40. M. Li, A. A. Beg, Induction of necrotic-like cell death by tumor necrosis factor alpha and caspase inhibitors: novel mechanism for killing virus-infected cells. *J. Virol.* **74**, 7470–7477 (2000).
41. A. L. McCormick, A. Skaletskaya, P. A. Barry, E. S. Mocarski, V. S. Goldmacher, Differential function and expression of the viral inhibitor of caspase 8-induced apoptosis (vICA) and the viral mitochondria-localized inhibitor of apoptosis (vMIA) cell death suppressors conserved in primate and rodent cytomegaloviruses. *Virology* **316**, 221–233 (2003).
42. K. Moriwaki, F. K.-M. Chan, The inflammatory signal adaptor RIPK3: functions beyond necroptosis. *Int. Rev. Cell Mol. Biol.* **328**, 253–275 (2017).
43. A. Louise McCormick, L. Roback, D. Livingston-Rosanoff, C. St Clair, The human cytomegalovirus UL36 gene controls caspase-dependent and-independent cell death programs activated by infection of monocytes differentiating to macrophages. *J. Virol.* **84**, 5108–5123 (2010).
44. S. Kang, *et al.*, Caspase-8 scaffolding function and MLKL regulate NLRP3 inflammasome activation downstream of TLR3. *Nat. Commun.* **6**, 7515 (2015).
45. S. A. Conos, *et al.*, Active MLKL triggers the NLRP3 inflammasome in a cell-intrinsic manner. *Proc. Natl. Acad. Sci.* **114**, E961–E969 (2017).
46. S. Yoon, A. Kovalenko, K. Bogdanov, D. Wallach, MLKL, the protein that mediates necroptosis, also regulates endosomal trafficking and extracellular vesicle generation. *Immunity* **47**, 51–65 (2017).
47. D. Frank, D. L. Vaux, J. M. Murphy, J. E. Vince, L. M. Lindqvist, Necroptotic MLKL

attenuates autophagy following its translocation to intracellular membranes. *J. Cell Sci.* **132** (2019).

48. I. Rusinova, *et al.*, INTERFEROME v2.0: an updated database of annotated interferon-regulated genes. *Nucleic Acids Res.* **41**, D1040–D1046 (2012).
49. C. M. Henry, S. J. Martin, Caspase-8 acts in a non-enzymatic role as a scaffold for assembly of a pro-inflammatory "FADDosome" complex upon TRAIL stimulation. *Mol. Cell* **65**, 715-729.e5 (2017).
50. M. Feoktistova, *et al.*, cIAPs block Ripoptosome formation, a RIP1/caspase-8 containing intracellular cell death complex differentially regulated by cFLIP isoforms. *Mol. Cell* **43**, 449–63 (2011).
51. T. Tenev, *et al.*, The Ripoptosome, a signaling platform that assembles in response to genotoxic stress and loss of IAPs. *Mol. Cell* **43**, 432–448 (2011).
52. J. L. Hartley, G. F. Temple, M. A. Brasch, DNA cloning using in vitro site-specific recombination. *Genome Res.* **10**, 1788–1795 (2000).
53. J. A. Vizcaíno, *et al.*, 2016 update of the PRIDE database and its related tools. *Nucleic Acids Res.* **44**, D447–D456 (2016).
54. J. Cox, M. Mann, MaxQuant enables high peptide identification rates, individualized p.p.b.-range mass accuracies and proteome-wide protein quantification. *Nat. Biotechnol.* **26**, 1367–1372 (2008).
55. L. V Nobre, *et al.*, Human cytomegalovirus interactome analysis identifies degradation hubs, domain associations and viral protein functions. *Elife* **8** (2019).
56. D. E. Christofferson, Y. Li, J. Yuan, Control of life-or-death decisions by RIP1 kinase. *Annu. Rev. Physiol.* **76**, 129–150 (2014).

FIGURES AND FIGURE LEGENDS

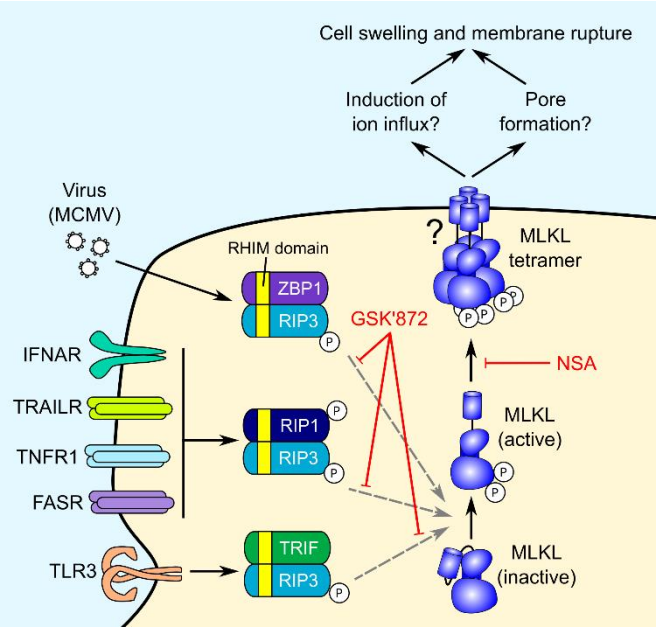

Figure 1. The necroptosis pathway and mechanism of action of small molecule necroptosis inhibitors. Two inhibitors of the necroptotic pathway were utilised in this study: GSK'872, which inhibits RIP3 kinase activity (31, 32), and necrosulfonamide (NSA), which inhibits downstream effector functions of MLKL via covalent reaction with human MLKL residue Cys^{86} (19, 33).

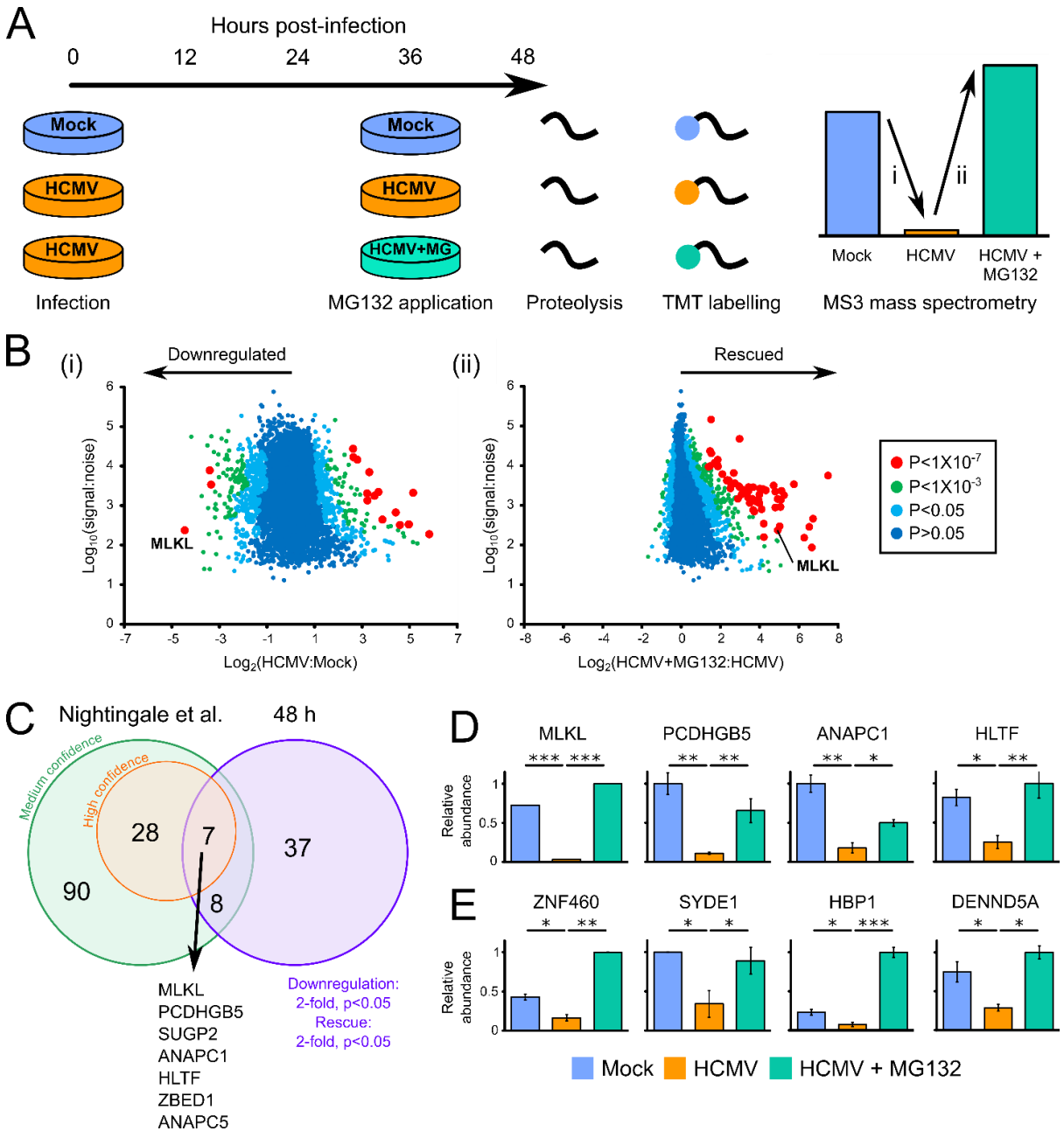

Figure 2. Identification of proteins targeted for degradation by HCMV at 48 hpi. (A) Schematic of the experimental method, conducted in biological duplicate. Cellular lysates from the second 48 h biological replicate were analysed simultaneously with residual lysates from the 12 h degradation screen in the Nightingale *et al.* study (10), facilitating a direct comparison **(SI Appendix, Figure S1A)**. Peptides from each sample were labelled with tandem mass tags and analysed by MS3 mass spectrometry. **(B)** Scatterplots of human proteins quantified at 48 hpi in one or both replicates, showing averaged ratios. P-values were estimated using significance B values, then corrected for multiple hypothesis testing (54). K-means clustering suggested there were at least nine different patterns of protein expression across the samples **(Dataset S1C and SI Appendix, Figure S1B)**. **(C)** Overlap between early degradation data from the Nightingale *et al.* study (using either stringent or sensitive

statistical criteria) (10) and 48 h degradation data presented in this study. **(D)** Examples of the seven proteins degraded with high confidence both early and late during infection. MLKL was only quantified in one replicate. Error bars: range. P-values were calculated as described in (B). *$p<0.05$, **$p<0.001$, ***$p<1\times10^{-7}$. Additional proteins were likely to have been degraded both early and late during infection **(Dataset S1 and SI Appendix, Figure S1A)**, but did not pass the stringent filtering criteria used at one or other of the time points. **(E)** Examples of the 37 proteins degraded at 48 h that were not confidently degraded at early time points. These comprised: (i) proteins not degraded at early time points (shown in this figure), (ii) proteins that were insufficiently degraded at early time points to pass filtering criteria, and (iii) proteins not quantified in the Nightingale *et al.* study (10). Additional examples and the corresponding 12 h data are shown in **Figure S1A (SI Appendix)**.

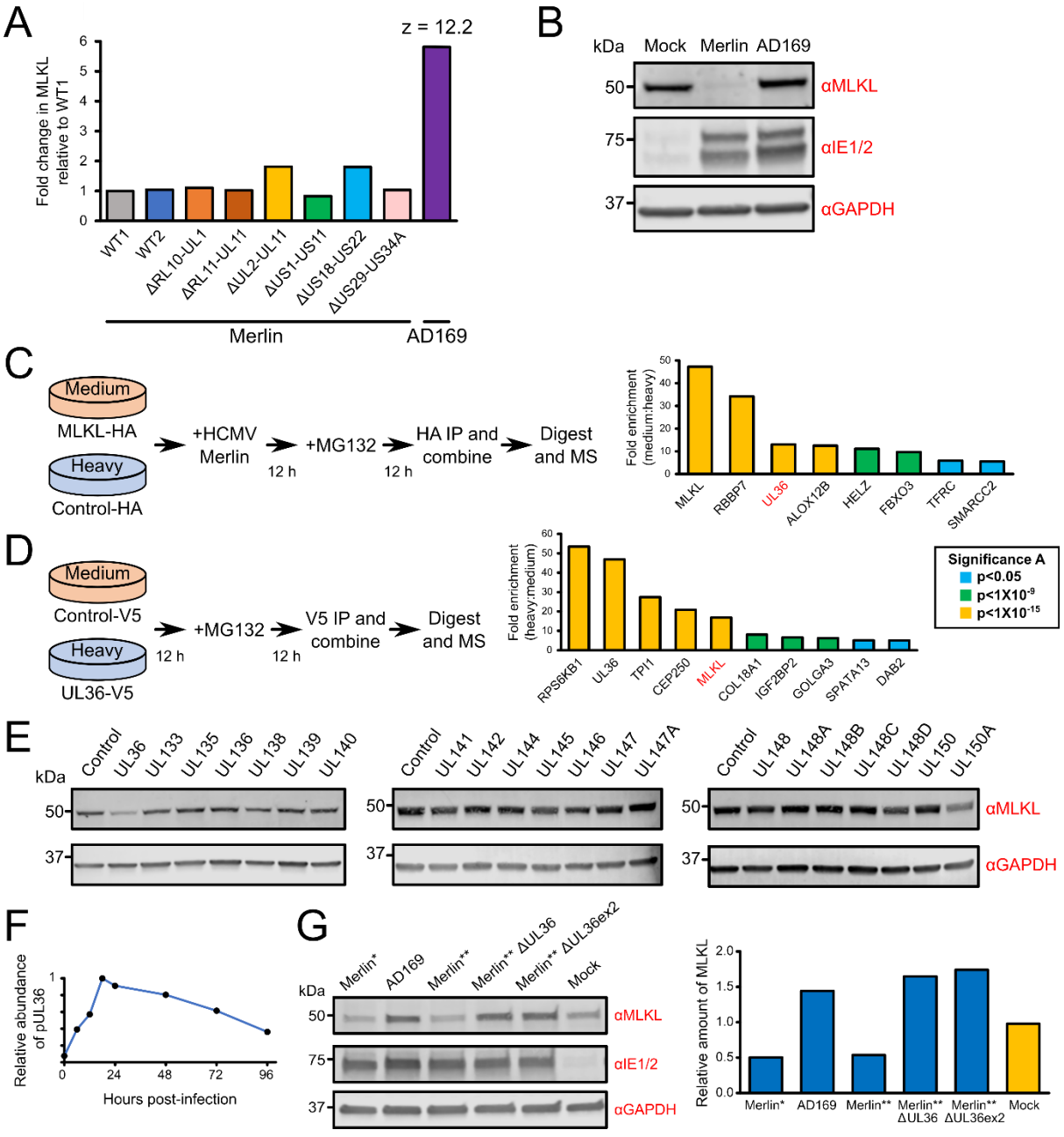

Figure 3. HCMV strain Merlin pUL36 is necessary and sufficient to degrade MLKL. (A) Relative abundance of MLKL from a proteomic screen of >250 proteins published in the Nightingale *et al*. study (10). HFFF-TERTs were infected with strain Merlin (WT1), WT1 that lacked UL16 and UL18 (WT2), one of six block-deletion viruses derived from WT1 or WT2, or strain AD169 (MOI = 10, 72 h infection). A z-score of >5 was considered significant. **(B)** Immunoblot confirming that MLKL is downregulated by strain Merlin but not by strain AD169 (MOI = 5, 48 h infection, cells lysed in RIPA buffer). MLKL was similarly downregulated in cells lysed in 2% SDS **(SI Appendix, Figure S2E)**. This was consistent with the observed MLKL downregulation in cells lysed with 6 M guanidine for proteomic experiments (**Figure 2**), and indicated that MLKL was likely degraded as opposed to being translocated to RIPA-insoluble membrane-associated complexes. **(C)** SILAC immunoprecipitation of

C-terminally HA-tagged MLKL or control in the presence of strain Merlin infection (MOI = 3, 24 h infection in the presence of 10 μM MG132 for the final 12 h). Proteins enriched >5-fold are shown. P-values were estimated using the method of significance A and corrected for multiple hypothesis testing (54). **(D)** SILAC immunoprecipitation of C-terminally V5-tagged pUL36 or control in the presence of 10 μM MG132 for 12 h. Proteins that were enriched >5-fold are shown, and p-values were estimated as described in (C). **(E)** Immunoblot showing that pUL36 is sufficient to downregulate MLKL. A series of HFFF-TERT cell lines stably expressing genes in the UL133-150A region were lysed in RIPA buffer and analysed by immunoblotting. Confirmation of viral protein expression was achieved by immunoblotting or mass spectrometry (55) (**Dataset S3D and SI Appendix, Figure S2B)**, except for pUL136, which was not detected by either method. MLKL was similarly downregulated by pUL36 in cells lysed in 2% SDS (**SI Appendix, Figure S2F**, as shown during HCMV infection in **Figure S2E)**. **(F)** Temporal profile of strain Merlin pUL36 in whole-cell lysates harvested at different times over the whole course of infection, from the Weekes *et al.* study (11). **(G)** Immunoblot showing that pUL36 is necessary for downregulation of MLKL (MOI = 5, 24 h infection). Cells were infected with WT strain Merlin (Merlin*), a version of Merlin in which intact genes UL128 and RL13 are under tet regulation (Merlin**), two UL36 deletion viruses derived from Merlin**, or strain AD169. ΔUL36ex2 has a deletion in exon 2. Right panel: the relative amount of MLKL normalised to GAPDH. Overall this data suggests that pUL36 is necessary and sufficient to degrade MLKL.

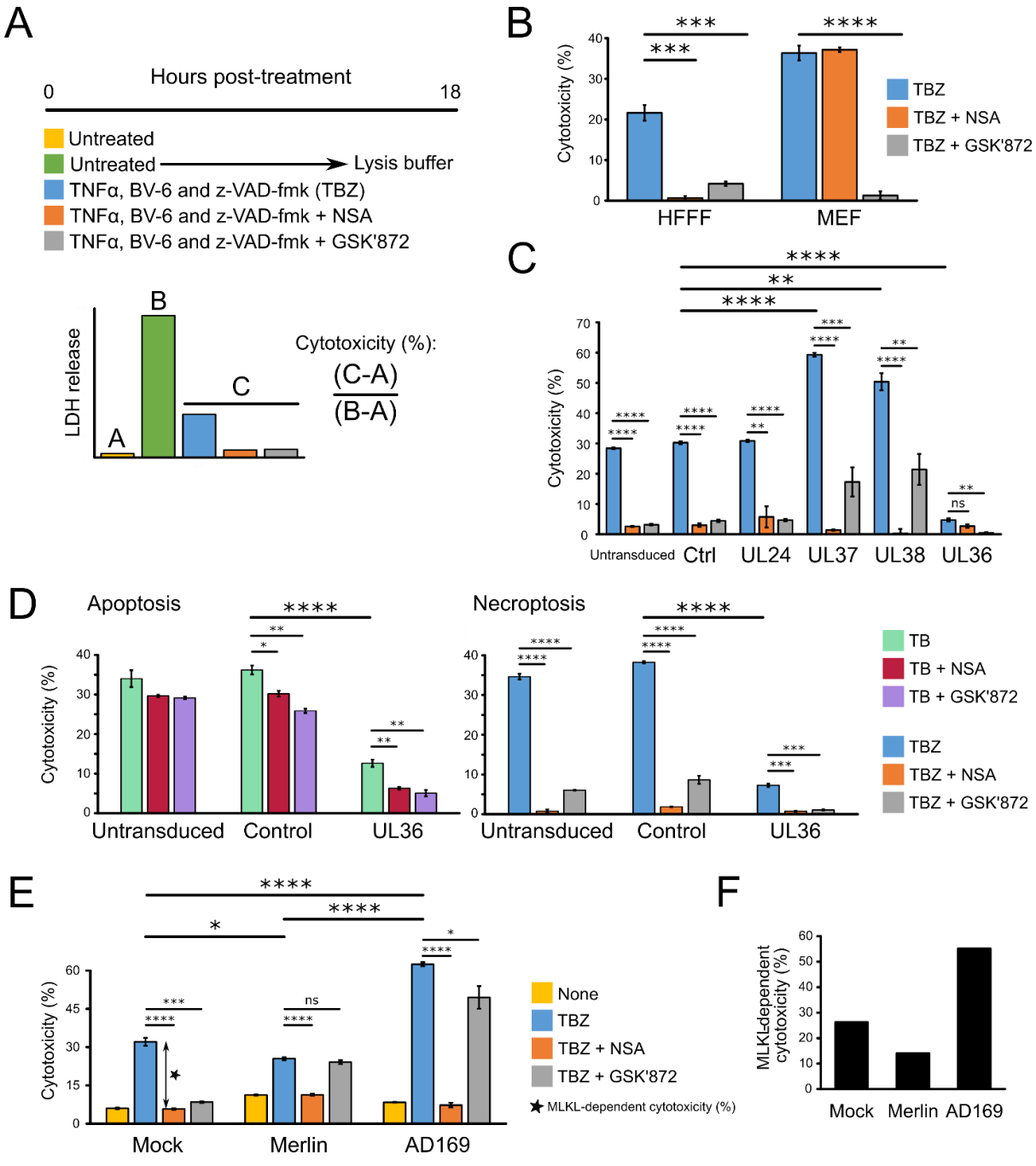

Figure 4. Role of MLKL degradation in HCMV infection. (A) Schematic of the necroptosis assay, which was performed in biological triplicate conducted in parallel and repeated in two or three completely independent experiments. Cytotoxicity was quantified by measuring lactate dehydrogenase (LDH) release using the CytoTox 96® Non-Radioactive Cytotoxicity Assay (Promega). Cytotoxicity was calculated as a percentage of 100% lysis (from untreated cells lysed with lysis buffer) after subtraction of background LDH release from live cells. To stimulate apoptosis, cells were treated with TB instead of TBZ. **(B)** TBZ induces MLKL- and RIP3-dependent necroptosis, which was inhibitable by GSK'872 in HFFF-TERTs and MEFs. NSA inhibited necroptosis in HFFF-TERTs but not MEFs, likely because NSA does not inhibit murine forms of MLKL (19). Error bars show standard error of the

mean (SEM). P-values were estimated using a two-tailed t-test (n=3). ***p < 0.001, ****p < 0.0001. Data are representative of three independent experiments. To dissect fully the conditions of this assay, stimulation with each of T, B and Z alone or in combination was examined in the presence or absence of inhibitors **(SI Appendix, Figures S4B-C)**. HFFFs were insensitive to T or Z alone, TZ or BZ. Cell death was stimulated by B alone in the absence of death receptor stimulation, an effect that has been observed in other cell types (56) **(SI Appendix, Figure S4B)**. The cell death initiated by BV6 was MLKL- and RIP3-independent, but also caspase-8-dependent (inhibited by the addition of Z), suggesting that BV6 alone was not responsible for the necroptotic cell death observed in the TBZ condition **(SI Appendix, Figures S4B-C)**. Collectively, these results suggest that only in the presence of TBZ was cell death dependent on MLKL and RIP3. **(C)** pUL36 is sufficient to inhibit necroptosis in stably transduced HFFF-TERTs treated with TBZ ± inhibitors. In addition to untransduced cells, two control vectors were employed. 'Ctrl' cells were transduced with a vector containing a short, randomised DNA sequence. pUL24 was included as a control HCMV tegument protein that has a similar size to pUL36 but lacks any known role in cell death. Error bars: SEM. P-values were estimated using a two-tailed t-test (n=3). **p < 0.01, ***p < 0.001, ****p < 0.0001. Data are representative of two independent experiments. **(D)** pUL36 inhibits both apoptosis and necroptosis. Untransduced, control or pUL36-expressing HFFF-TERTs were treated for 18 h with either TB or TBZ to stimulate apoptosis or necroptosis, respectively, in the presence or absence of NSA or GSK'872. Error bars: SEM. P-values were estimated using a two-tailed t-test (n=3). *p < 0.05, **p < 0.01, ***p < 0.001, ****p < 0.0001. Data are representative of two independent experiments. **(E)** Functional pUL36 was required for inhibition of necroptosis, comparing 48 h mock, Merlin or AD169 infection (MOI = 5) in HFFF-TERTs subsequently stimulated with TBZ ± inhibitors for 18 h. Baseline cytotoxicity in untreated cells was not subtracted from the other values and is shown as a separate yellow bar. Error bars: SEM. P-values were estimated using a two-tailed t-test (n=3). *p < 0.05, ***p < 0.001, ****p < 0.0001. Data are representative of two independent experiments. **(F)** MLKL-dependent cytotoxicity was calculated from the difference between % cytotoxicity (TBZ alone) versus (TBZ+NSA), shown by the double-headed arrow in **Figure 4E**.

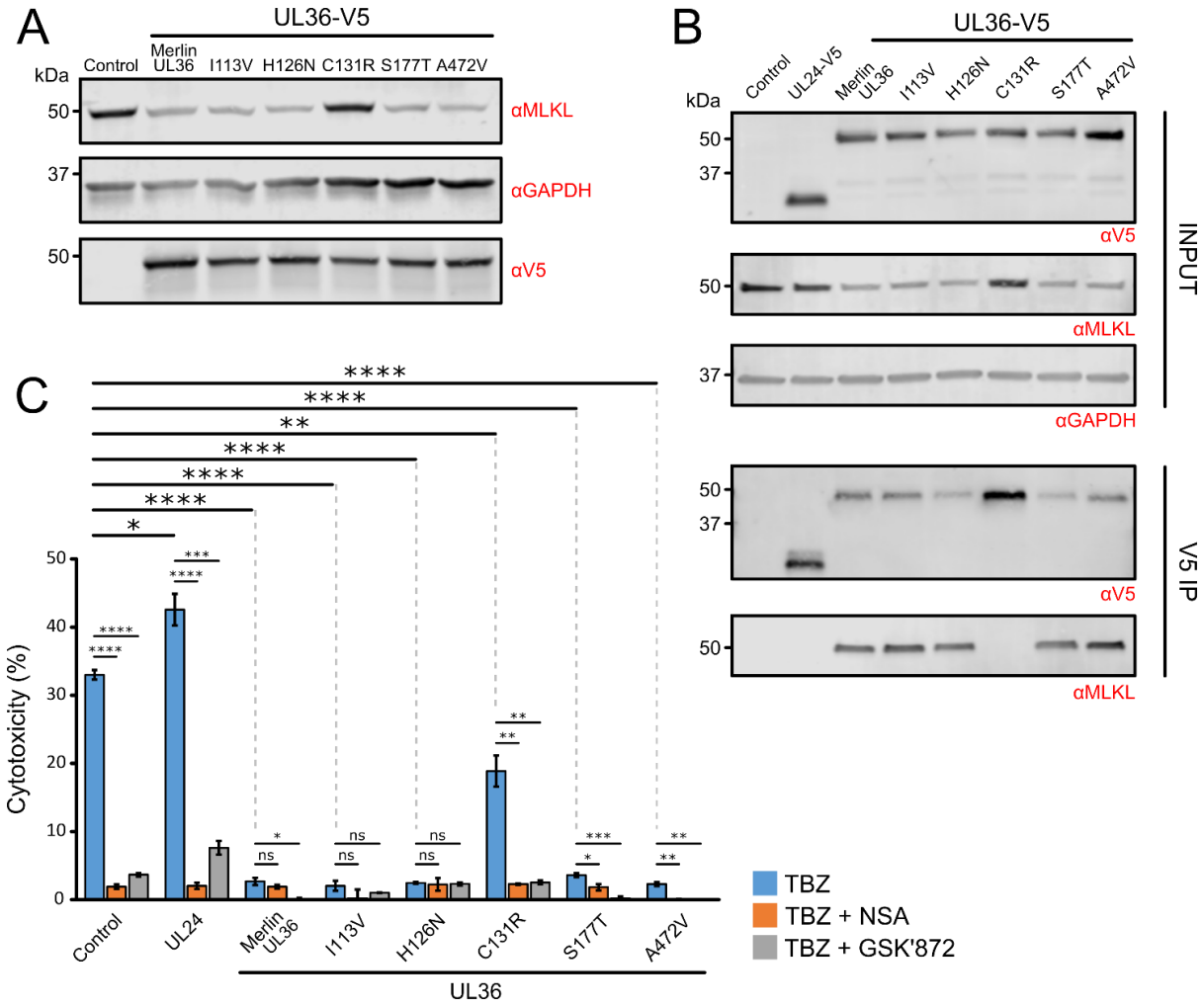

Figure 5. Substitution of Cys[131] in strain Merlin pUL36 abrogates binding to and degradation of MLKL, and inhibition of necroptosis. (A) Immunoblot showing that downregulation of MLKL is dependent on the pUL36 Cys[131] residue. HFFF-TERTs were stably transduced with the indicated C-terminally V5-tagged UL36 constructs. Individual point mutations corresponding to the five amino acid substitutions between strain Merlin and strain AD169 pUL36 are shown above the blot and detailed in **Figure S5 (SI Appendix)**. **(B)** Interaction between pUL36 and MLKL is dependent on pUL36 Cys[131], shown by a V5 co-IP in the cell lines described in (A). Immunoblots were probed with anti-V5, anti-MLKL and anti-GAPDH antibodies. **(C)** Percentage cytotoxicity of cell lines described in (A) that were treated with TBZ ± NSA or GSK'872. Error bars: SEM. P-values were estimated using a two-tailed t-test (n=3). *p<0.05, **p < 0.01, ***p < 0.001, ****p< 0.0001. Data are representative of two independent experiments. Low-level variation in sensitisation to necroptosis was observed between the unmodified, control and UL24-expressing cell lines (comparing data in this figure to **Figure 4C**).

PNAS
www.pnas.org

Supplementary Information for

Human cytomegalovirus protein pUL36: a dual cell death pathway inhibitor

Alice Fletcher-Etherington[a], Luis Nobre[a], Katie Nightingale[a], Robin Antrobus[a], Jenna Nichols[b], Andrew J. Davison[b], Richard J. Stanton[c], Michael P. Weekes[a,1]

Affiliations:
a Cambridge Institute for Medical Research, University of Cambridge, Hills Road, Cambridge CB2 0XY, UK
b MRC-University of Glasgow Centre for Virus Research, Sir Michael Stoker Building, 464 Bearsden Road, Glasgow G61 1QH, UK
c Cardiff University School of Medicine, Division of Infection and Immunity, Henry Wellcome Building, Heath Park, Cardiff CF14 4XN, UK
1 Corresponding author

Correspondence:
Michael P. Weekes
Email: mpw1001@cam.ac.uk

This PDF file includes:

Supplementary text (Materials and Methods)
Figures S1 to S5
Legends for Datasets S1 to S3
SI References

Other supplementary materials for this manuscript include the following:

Datasets S1 to S3

Supplementary Information Text

Materials and Methods

Cells and cell culture

All fibroblast cell lines generated in this paper were derived from human foetal foreskin fibroblasts immortalised with human telomerase (HFFF-TERTs) (1). HFFF-TERTs have been tested at regular intervals since isolation to confirm that human leukocyte antigen (HLA) and MHC Class I Polypeptide-Related Sequence A (MICA) genotypes, cell morphology and antibiotic resistance are unchanged. HFFF-Tets (used for growing tet-regulated viruses) additionally constitutively expressed the tetracycline (tet) repressor. Mouse embryonic fibroblasts (MEFs) immortalised with SV40 large T antigen were kindly provided by Dr Evan Reid (University of Cambridge) and are described in the Allison *et al.* study (2). HEK293T cells used for generation of lentivirus were obtained as a gift from Professor Paul Lehner (University of Cambridge). All cells were grown at 37 °C in 5 % v/v CO_2 in Dulbecco's modified Eagle's medium (DMEM) supplemented with foetal bovine serum (FBS: 10% v/v), and 100 IU/ml penicillin / 0.1 mg/ml streptomycin (DMEM/FBS/PS). For SILAC immunoprecipitations (IPs), cells were grown for seven passages in SILAC DMEM (Gibco), which was supplemented with 10% dialysed FBS (Gibco), penicillin/streptomycin, 280 mg/l L-proline (Sigma-Aldrich), and either medium (Arg 6, Lys 4) or heavy (Arg 10, Lys 8) amino acids (CK Isotopes) at 50 mg/ml.

Viruses

The genome sequence of HCMV strain Merlin (GenBank accession AY446894) is designated the reference HCMV sequence (RefSeq accession NC_006273.2) by the National Center for Biotechnology Information (3, 4). A recombinant version (RCMV1111) of this strain was derived by transfection of a sequenced BAC clone (4). RCMV1111 contains point mutations in two genes (RL13 and UL128) that enhance replication in fibroblasts (4). The block HCMV deletion mutants are described in the Nightingale *et al.* study (5). The AD169-GFP virus (RCMV288) is described in the McSharry *et al.* study (1). RCMV1502 is an RCMV1111 recombinant that has tet-operators 5' to the RL13 and UL128 coding sequences (Merlin-$RL13_{tetO}$-$UL128_{tetO,}$) and is described in the Stanton *et al.* study (4). UL36 deletion mutants were generated by recombineering RCMV1502 (4). Two deletion mutants were generated, one lacking the whole UL36 coding sequence (ΔUL36; RCMV2288), and the other lacking the second UL36 exon (ΔUL36ex2; RCMV2289). Virus stocks were prepared in HFFF-TERTs or HFFF-Tets (for tet-regulated viruses) as described in the Stanton

et al. study (6). Whole-genome consensus sequences of passage 1 of each RCMV were determined using the Illumina platform as described previously (7).

Viral infections

The required volume of viral stock to achieve the multiplicity of infection (MOI) described in the results section was diluted in serum-free DMEM, mixed gently and applied to HFFF-TERTs. Mock infections were performed identically but with DMEM instead of viral stock. Time zero was considered the time at which cells first came into contact with virus. Cells were incubated with virus for 2 h at 37 °C on a rocking platform, and then the medium was replaced with DMEM/FBS.

Proteomic Screen

The 48 h degradation screen in this paper was performed in biological duplicate. Cellular lysates from the second 48 h biological replicate were analysed simultaneously with residual lysates from the 12 h degradation screen in the Nightingale *et al.* study (5), thus facilitating a direct comparison.

Infection

In **Experiment 1**, 3×10^6 HFFF-TERTs were plated in DMEM/FBS/PS in 75 cm^2 flasks. After 24 h, the medium was replaced by serum-free DMEM containing 4 µg/ml dexamethasone, which has been shown to improve infection efficiency (8, 9). After a further 24 h, the medium was removed and the cells were infected as described above at an MOI of 10. At 36 hours post-infection (hpi), 10 µM MG132 (Merck) or the equivalent volume of DMSO (Sigma-Aldrich) was added to the cells. In **Experiment 2**, 8×10^5 HFFF-TERTs were seeded into 25 cm^2 flasks, and then treated as in Experiment 1.

Whole Cell Lysate Protein Digestion

Methods for whole cell lysate protein preparation and digestion, peptide labelling with tandem mass tags, HpRP fractionation, liquid chromatography-mass spectrometry and data analysis are discussed in detail in the Nightingale *et al.* study (5), and are recapitulated below including modifications for the present study.

At 48 hpi, cells were washed twice with PBS, and 500 µl lysis buffer was added (6 M guanidine/50 mM HEPES pH 8.5). Cell lifters (Corning) were used to scrape the cells into lysis buffer, which was then removed to an eppendorf tube, vortexed extensively and sonicated. Cell debris was removed by centrifuging twice at 21,000 g for 10 min.

From this point onward, lysates from the second biological replicate (Experiment 2) were treated identically to residual lysates from a 12 h degradation screen that we performed previously (5). Dithiothreitol (DTT) was added to a final concentration of 5 mM and incubated at room temperature for 20 mins. Cysteine residues were alkylated with 15 mM iodoacetamide and incubated for 20 min at room temperature in the dark. Excess iodoacetamide was quenched with DTT for 15 mins. Samples were diluted with 200 mM HEPES pH 8.5 to 1.5 M guanidine followed by digestion at room temperature for 3 h with LysC protease at a 1:100 protease-to-protein ratio. Samples were further diluted with 200 mM HEPES pH 8.5 to 0.5 M guanidine. Trypsin was then added at a 1:100 protease-to-protein ratio followed by overnight incubation at 37°C. The reaction was quenched with 5% formic acid and centrifuged at 21,000 g for 10 min to remove undigested protein. Peptides were subjected to C18 solid-phase extraction (SPE, Sep-Pak, Waters) and vacuum-centrifuged to near-dryness.

Peptide Labelling with Tandem Mass Tags

In preparation for TMT labelling, desalted peptides were dissolved in 200 mM HEPES pH 8.5. Peptide concentration was measured by microBCA (Pierce), and 25 µg of peptide was labelled with TMT reagent. TMT reagents (0.8 mg, Thermo Scientific) were dissolved in 43 µl anhydrous acetonitrile and 3 µl were added to each peptide sample at a final acetonitrile concentration of 30% (v/v). Samples were labelled as follows: **Experiment 1:** 48 h mock (TMT 128N), 48 h infection (TMT 129N), 48 h infection / MG132 (TMT 130C). **Experiment 2:** 12 h mock (TMTpro 126), 12 h infection (TMTpro 127C), 12 h infection / MG132 (TMTpro 128N), 48 h mock (TMTpro 131C), 48 h infection (TMTpro 132C), 48 h infection / MG132 (TMTpro 133N). Following incubation at room temperature for 1 h, the reaction was quenched with hydroxylamine to a final concentration of 0.5% (v/v). TMT-labelled samples were combined at a 1:1:1 ratio (**Experiment 1**) or 1:1:1:1:1:1 ratio (**Experiment 2**). The sample was vacuum-centrifuged to near dryness and subjected to C18 SPE (Sep-Pak, Waters). An unfractionated single-shot was analysed initially to ensure similar peptide loading across each TMT channel, thus avoiding the need for excessive electronic normalisation. In **Experiment 1**, data from the single-shot experiment was analysed with data from the corresponding fractions to increase the overall number of peptides quantified. In **Experiment 2**, data from 13 fractions were used in the analysis. Normalisation is discussed in 'Data Analysis' and high pH reversed-phase (HpRP) fractionation is discussed below.

Offline HpRP Fractionation

TMT-labelled tryptic peptides were subjected to HpRP fractionation using an Ultimate 3000 RSLC UHPLC system (Thermo Fisher Scientific) equipped with a 2.1 mm internal diameter (ID) x 25 cm long, 1.7 µm particle Kinetix Evo C18 column (Phenomenex). Mobile phase consisted of A: 3% acetonitrile (MeCN), B: MeCN, and C: 200 mM ammonium formate pH 10. Isocratic conditions were 90% A/10% C, and C was maintained at 10% throughout the gradient elution. Separations were conducted at 45 °C. Samples were loaded at 200 µl/minute for 5 min. The flow rate was then increased to 400 µl/minute over 5 minutes, after which the gradient elution proceeded as follows: 0-19% B over 10 minutes, 19-34% B over 14.25 minutes, 34-50% B over 8.75 minutes, followed by a 10 min wash at 90% B. UV absorbance was monitored at 280 nm and 15 s fractions were collected into 96 well microplates using the integrated fraction collector. Fractions were recombined orthogonally in a checkerboard fashion, combining alternate wells from each column of the plate into a single fraction, and commencing combination of adjacent fractions in alternating rows. Wells were excluded prior to the start or after the cessation of elution of peptide-rich fractions, as identified from the UV trace. This yielded two sets of 12 combined fractions, A and B, which were dried in a vacuum centrifuge and resuspended in 10 µl MS solvent (4% MeCN/5% formic acid) prior to LC-MS3. 12 set 'A' fractions were used for MS analysis for **Experiment 1** and 12 set 'A' and one set 'B' fractions were used for **Experiment 2**.

LC-MS3

For **Experiment 1,** mass spectrometry data were acquired using an Orbitrap Fusion mass spectrometer (Thermo Fisher Scientific, San Jose, CA). Peptides were separated using a Proxeon EASY-nLC 1000 LC pump equipped with a 75 µm inner diameter microcapillary column packed with 0.5 cm of Magic C4 resin (5 µm, 100 Å, Michrom Bioresources) followed by ~20 cm of GP118 resin (1.8 µm, 120 Å, Sepax Technologies). Peptides were separated using a 3 hr gradient of 6-30% acetonitrile in 0.125% formic acid at a flow rate of 300 nL/min. Each analysis used a MultiNotch MS3-based TMT method (10, 11). The following settings were used: MS1: 400-1400 Th, Quadrupole isolation, 120,000 Resolution, 2×10^5 AGC target, 100 ms maximum injection time, ions injected for all parallisable time. MS2: Quadrupole isolation at an isolation width of m/z 0.5, CID fragmentation (NCE 35) with ion trap scanning out in rapid mode from m/z 350, 4000 AGC target, 150 ms maximum injection time, in centroid mode. MS3: In Synchronous Precursor Selection mode, the top 10 MS2 ions were selected for HCD fragmentation (NCE 55) and scanned in the Orbitrap at 60,000 resolution with an AGC target of 5×10^4 and a maximum accumulation time of 150 ms. Ions were not accumulated for all parallelisable time. The entire MS/MS/MS cycle

had a target time of 3 s. Dynamic exclusion was set to +/- 7 ppm for 90 s. MS2 fragmentation was trigged on precursors 5×10^3 counts and above.

For **Experiment 2,** mass spectrometry data were acquired using an Orbitrap Lumos (Thermo Fisher Scientific, San Jose, CA). An Ultimate 3000 RSLC nano UHPLC equipped with a 300 µm ID x 5 mm Acclaim PepMap µ-Precolumn (Thermo Fisher Scientific) and a 75 µm ID x 50 cm 2.1 µm particle Acclaim PepMap RSLC analytical column was used. Loading solvent was 0.1% formic acid (FA), analytical solvent A: 0.1% FA and B: 80% MeCN + 0.1% FA. All separations were carried out at 40°C. Samples were loaded at 5 µl/min for 5 min in loading solvent before beginning the analytical gradient. The following gradient was used: 3-7% B over 3 min, 7-37% B over 173 min, followed by a 4 min wash at 95% B and equilibration at 3% B for 15 min. Each analysis used a MultiNotch MS3-based TMT method (10, 11). The following settings were used: MS1: 380-1500 Th, 120,000 Resolution, 2×10^5 automatic gain control (AGC) target, 50 ms maximum injection time. MS2: Quadrupole isolation at an isolation width of m/z 0.7, CID fragmentation (normalised collision energy (NCE) 34) with ion trap scanning in turbo mode from m/z 120, 1.5×10^4 AGC target, 120 ms maximum injection time. MS3: In Synchronous Precursor Selection mode the top 10 MS2 ions were selected for HCD fragmentation (NCE 45) and scanned in the Orbitrap at 60,000 resolution with an AGC target of 1×10^5 and a maximum accumulation time of 150 ms. Ions were not accumulated for all parallelisable time. The entire MS/MS/MS cycle had a target time of 3 s. Dynamic exclusion was set to ± 10 ppm for 70 s. MS2 fragmentation was trigged on precursors 5×10^3 counts and above.

Immunoblotting

For the majority of immunoblots in this study, cells were lysed in RIPA buffer (Cell Signalling Technology) containing cOmplete EDTA-free Protease Inhibitor Cocktail (Roche) for 15 minutes at 4°C. For **Figures S2E and S2F**, cells were lysed in 2% SDS in PBS supplemented with 2.5 U/µl benzonase (Sigma) for 30 minutes at 37°C. Supernatants were sonicated and clarified by centrifugation at 14,000 g for 10 minutes. A Bicinchoninic Acid (BCA) assay (Pierce) was used to measure protein concentration according to the manufacturer's instructions. Samples were denatured and reduced with 6× Protein Loading Dye (375 mM Tris pH 6.8, 12% SDS, 30% glycerol, 0.6 M DTT, 0.06% bromophenol blue) for 5 minutes at 95°C. 40 µg (except **Figure 5A**; 50 µg and **Figure S2E**; 20 µg) of protein was separated by SDS-polyacrylamide gel electrophoresis (SDS-PAGE) using Mini-PROTEAN TGX precast gels (Bio-Rad), then transferred to polyvinylidene difluoride (PVDF) membranes (0.45 µm pore) using the Bio-Rad Trans-Blot system. The following primary antibodies were used: anti-MLKL (Cell Signalling Technology,

14993S, 1:1000), anti-IE1/2 (Abcam, ab53495, 1:1000), anti-GAPDH (R&D Systems, MAB5718, 1:10,000), anti-V5 (Invitrogen, R960-25, 1:2000). Secondary antibodies used were IRDye 680RD goat anti-mouse (LI-COR, 925-68070, 1:10,000) and IRDye 800CW goat anti-rabbit (LI-COR, 925-32211, 1:10,000). Fluorescent signals were detected using the Odyssey CLx Imaging System (LI-COR), and images were processed and quantified using Image Studio Lite V5.2 (LI-COR).

Plasmid construction

Generation of lentiviral expression vectors

cDNA was generated from HFFF-TERTs by reverse transcription of RNA using an RNeasy Mini Kit (Qiagen) followed by GoScript Reverse Transcriptase (Promega) according to the manufacturer's protocol. To generate an expression construct for MLKL-HA, primers were designed to recognise the 3' and 5' ends of the MLKL gene and contained flanking Gateway attB sequences to facilitate cloning into pDONR223 using the Gateway system (Thermo Scientific). The reverse primer additionally contained a 6 bp linker region, followed by the coding sequence for an HA tag and a stop codon **(Dataset S3A)**.

For expression of the V5-tagged viral genes, recombinant adenovirus vectors (RAds) were used as a template as described previously (9). Each template expressed a C-terminally V5-tagged gene under the control of the HCMV major immediate early promoter, with a 6 bp linker region between the end of the gene and the tag. To amplify genes from the RAds, primers were designed to recognise the 3' end of the HCMV promoter (forward 'GAW-CMVp-F') and the 3' end of the V5 tag (reverse 'attB2-V5-R') **(Dataset S3A)**. Both primers had flanking Gateway attB sequences. Spliced UL150A was synthesized as double-stranded DNA fragment (gBlocks®, Integrated DNA Technologies) comprising the viral gene succeeded by a 6 bp linker region, the coding sequence for the V5 tag and then the stop codon, and Gateway attB sequences.

PCR amplification of MLKL-HA and the viral genes was achieved using PfuUltra II fusion HS DNA polymerase (Agilent). PCR products were subsequently purified using a QIAquick Gel Extraction Kit (Qiagen), cloned into the pDONR223 entry vector, and then into the lentiviral destination vector pHAGE-pSFFV (described in the Nightingale *et al.* study (5)) (12). The sequence of MLKL was confirmed as the long, necroptotic isoform and shown to contain two non-disease-causing natural variants (S52T and M169L); this and the confirmed sequences of HCMV genes used in this study are shown in **Dataset S3B**. The UL36 gene sequence contains a single intron. Confirmation of splicing was achieved by reverse transcription of RNA from UL36-expressing

HFFF-TERTs and sequencing of the cDNA **(Dataset S3B)**. The pHAGE-SFFV control vector contains a short randomized DNA sequence (5).

All constructed plasmids were transformed into Alpha-Select Silver Efficiency Competent *E. coli* cells (Bioline) and selected on antibiotic-containing LB agar plates (pDONR223; spectinomycin, pHAGE-pSFFV; ampicillin).

PCR site-directed mutagenesis to generate UL36 point mutants

In the first round of PCR, two pairs of primers were used in two separate PCRs using strain Merlin UL36-V5 in the pDONR223 vector as a template. In the first reaction, reverse PCR primers encompassing each of the point mutants were combined with the UL36 attB1 fwd primer **(Dataset S3C)**. In the second reaction, forward PCR primers encompassing each of the point mutants were combined with the UL36 V5 attB2 rev primer **(Dataset S3C)**. A second round of PCR joined the two halves of UL36 by using the UL36 attB1 fwd and UL36 V5 attB2 rev primers. Five resulting PCR products encoding each of the different point mutants flanked by attB sites were cloned into pDONR223 and then pHAGE-pSFFV by Gateway cloning, and the sequences were confirmed.

Stable cell line production

Lentiviral particles were generated through transfection of HEK293T cells with the lentiviral expression vector and two helper plasmids (VSVg and pCMV.DR8.91, both kindly provided by Professor Paul Lehner), using TransIT-293 (Mirus) according to the manufacturer's instructions. Viral supernatant was harvested 48 h after transfection and diluted to achieve ~30% transduction of target cells, and debris was removed using a 0.22 µM filter (Millipore). 48 h after transduction, cells were subjected to antibiotic selection. Expression of the viral proteins pUL36 and pUL133-pUL150A was confirmed by immunoblotting for the V5 tag or IP-MS (9) (see 'Immunoprecipitation') **(Dataset S3D)**.

Immunoprecipitation

Cells were harvested in lysis buffer (50 mM Tris pH 7.5, 300 mM NaCl, 0.5% (v/v) NP40, 1 mM DTT and cOmplete EDTA-free Protease Inhibitor Cocktail (Roche)), tumbled on a rotator for 15 minutes at 4 °C, and then centrifuged at 16,100 g for 15 minutes at 4 °C. Lysates were clarified by filtration through a 0.7 µm filter and incubated for 3 h with immobilised mouse monoclonal anti-V5 or anti-HA agarose resin (Sigma). Samples were washed multiple times with lysis buffer and PBS.

Sample preparation for proteomic analysis

Confirmation of expression of viral proteins and analysis of SILAC IP data were achieved by using LC-MS/MS. Proteins bound to the resin were eluted twice with 200 µl of 250 µg/ml V5 (Alpha Diagnostic International) or HA (Sigma-Aldrich) peptide in PBS at 37 °C for 30 minutes with agitation. For SILAC-labelled samples, the medium- and heavy-labelled samples were then combined. Proteins were precipitated with 20% Trichloroacetic acid (TCA), washed once with 10% TCA, washed three times with cold acetone and dried to completion. The proteins were then digested in digestion buffer (50 mM Tris-HCl pH 8.5, 10% acetonitrile, 1 mM DTT, 10 µg/ml trypsin) and incubated overnight at 37 °C with agitation. The digestion reaction was quenched with 50% FA, and the peptides were subjected to C18 solid-phase extraction and dried in a centrifugal vacuum. Samples were resuspended in 4% acetonitrile / 5% FA in HPLC grade water and analysed by mass spectrometry on the Orbitrap Lumos as described below.

LC-MS/MS for IP experiments

Mass spectrometry data were acquired using an Orbitrap Fusion mass spectrometer (Thermo Fisher Scientific, San Jose, CA). Peptides were separated using an Ultimate 3000 RSLC nano UHPLC equipped with a 300 µm ID x 5 mm Acclaim PepMap µ-Precolumn (Thermo Fisher Scientific) and a 75 µm ID x 50 cm 2.1 µm particle Acclaim PepMap RSLC analytical column. Peptides were separated using a 3 hr gradient of 3-37% acetonitrile in 0.125% formic acid at a flow rate of 250 nL/min. The following settings were used: MS1: 350-1500 Th, Quadrupole isolation, 120,000 Resolution, 2×10^5 AGC target, 50 ms maximum injection time, ions injected for all parallisable time. MS2: Quadrupole isolation at an isolation width of m/z 0.7, HCD fragmentation (NCE 34) with ion trap scanning out in rapid mode from m/z 120, 10000 AGC target, 250 ms maximum injection time, in centroid mode. Dynamic exclusion was set to +/- 10 ppm for 25 s. MS2 fragmentation was trigged on precursors 5×10^3 counts and above.

Sample preparation for immunoblotting

Proteins bound to the resin were eluted once with 40 µl 2.5 mg/ml V5 or HA peptide at 37 °C for 1 hour with agitation. Eluted proteins were reduced with 6× Protein Loading Dye (Tris 375 mM pH 6.8, 12% SDS, 30% glycerol, 0.6M DTT, 0.06% bromophenol blue) at 95 °C for 5 minutes prior to separation by SDS-PAGE as described above. For the input blot, 2% of the original lysates were removed prior to IP and heated in 6× Loading Dye at 95 °C for 5 minutes prior to SDS-PAGE.

Immunofluorescence

1.2×10^5 HFFF-TERTs were seeded onto 13 mm coverslips (VWR) in a 24-well plate and incubated overnight. Coverslips were washed in the well three times with PBS and then fixed with 4% paraformaldehyde Fixation Buffer (Bio-Rad) for 20 minutes at room temperature. Two more washes with PBS were followed by permeabilisation in 0.1% (v/v) Triton® X-100 (Thermo) / 2% (v/v) FBS in PBS for 4 minutes. Coverslips were then washed twice in each of blocking buffer (10% (v/v) FBS in PBS), PBS and ultrapure water, before blocking for 1 h. The primary antibodies were diluted in blocking buffer and incubated with the coverslips overnight at 4 °C. Coverslips were then washed in blocking buffer, PBS and water as before, and then incubated with secondary antibody in blocking buffer for 1 h. Coverslips were washed again as before, incubated with 1 µg/ml DAPI (Thermo Scientific) in water and washed again before mounting on slides with ProLong™ Gold antifade reagent (Thermo Scientific). The primary antibodies used were anti-HA (Cell Signalling Technology, 3724, 1:50) and anti-V5 (Thermo, MA5-15253, 1:1000). The secondary antibodies used were anti-mouse Alexa Fluor® 488 (Cell Signalling Technology, 4408S, 1:300) and anti-rabbit Alexa Fluor® 647 (Thermo, A31573, 1:300).

Cell death assays

All experiments were performed in biological triplicate conducted in parallel and repeated in 2 or 3 completely independent experiments. Input cell numbers and time of stimulation were optimised to ensure that sufficient cells died to facilitate quantitation of statistically significant differences between cell populations, and resulted in absorbance values within the dynamic range of the plate reader. *For assays in the absence of infection,* 96-well plates were seeded with HFFF-TERTs (18,000 cells/well) or immortalised MEFs (6,000 cells/well) then incubated for 24 h. For test cells, the medium was changed to DMEM supplemented with 5% v/v FBS, 30 ng/ml TNFα (R&D systems), 5 µM BV-6 (Selleckchem), or 25 µM z-VAD-fmk (BD Pharmingen) in the presence or absence of 0.5 µM necrosulfonamide (NSA, Merck) or 1.5 µM GSK'872 (Cayman Chemical) for 18 h. Each compound was solubilised in DMSO, and DMSO was added such that its final concentration in each experimental condition was the same. For control cells, the medium was changed to DMEM supplemented with an equivalent concentration of DMSO. 45 mins prior to harvest, half of the control cells were treated with 10 µl 10X Lysis Solution (Promega) to observe lactate dehydrogenase (LDH) release from maximally lysed cells. The other half were used to measure background LDH release from live, untreated cells. Supernatants were harvested and the release of LDH was measured using the CytoTox 96 Non-Radioactive Cytotoxicity Assay (Promega). Average absorbance values derived from culture medium alone were subtracted from

each absorbance value from experimental wells. *For assays in the presence of infection*, HFFF-TERTs (14,000 cells/well) were seeded into 96-well plates, incubated for 24 h, and infected with HCMV (MOI = 5). 48 h after infection, the medium was changed as described above to generate populations of cells stimulated for necroptosis, or control cells.

Quantification and Statistical Analysis

Data Analysis

Mass spectra were processed using a Sequest-based software pipeline for quantitative proteomics, ''MassPike'', through a collaborative arrangement with Professor Steven Gygi's laboratory at Harvard Medical School. MS spectra were converted to mzXML using an extractor built upon Thermo Fisher's RAW File Reader library (version 4.0.26). In this extractor, the standard mzxml format has been augmented with additional custom fields that are specific to ion trap and Orbitrap mass spectrometry and essential for TMT quantitation. These additional fields include ion injection times for each scan, Fourier Transform-derived baseline and noise values calculated for every Orbitrap scan, isolation widths for each scan type, scan event numbers and elapsed scan times. This software is a component of the MassPike software platform and is licensed by Harvard Medical School. A combined database was constructed from (a) the human Uniprot database (26th January, 2017), (b) the HCMV strain Merlin Uniprot database, (c) all additional non-canonical HCMV ORFs described by Stern-Ginossar *et al.* (13), (d) a six-frame translation of HCMV strain Merlin filtered to include all potential ORFs of ≥8 amino acids (delimited by stop-stop rather than requiring ATG-stop) and (e) common contaminants such as porcine trypsin and endoproteinase LysC. ORFs from the six-frame translation (6FT-ORFs) were named as follows: 6FT_Frame_ORFnumber_length, where Frame is numbered 1-6, and length is the length in amino acids. The combined database was concatenated with a reverse database composed of all protein sequences in reversed order. Searches were performed using a 20 ppm precursor ion tolerance. Fragment ion tolerance was set to 1.0 Th. TMT tags on lysine residues and peptide N termini (**Experiment 1:** 229.162932 Da; **Experiment 2:** 304.2071) and carbamidomethylation of cysteine residues (57.02146 Da) were set as static modifications, while oxidation of methionine residues (15.99492 Da) was set as a variable modification. Where indicated, data were re-searched using phosphorylation (79.96633 Da) of serine, threonine or tyrosine residues as an additional variable modification. For SILAC analysis, the following variable modifications were used: heavy lysine (8.01420 Da), heavy arginine (10.00827 Da), medium lysine (4.02511 Da), and medium arginine (6.02013 Da). SILAC-only searches were performed in the same manner, omitting the TMT static modification. To control the fraction of erroneous protein identifications, a target-decoy strategy was employed (14). Peptide

spectral matches (PSMs) were filtered to an initial peptide-level false discovery rate (FDR) of 1% with subsequent filtering to attain a final protein-level FDR of 1%. PSM filtering was performed using a linear discriminant analysis, as described previously (14). This distinguishes correct from incorrect peptide IDs in a manner analogous to the widely used Percolator algorithm (https://noble.gs.washington.edu/proj/percolator/), though employing a distinct machine-learning algorithm. The following parameters were considered: XCorr, DCn, missed cleavages, peptide length, charge state, and precursor mass accuracy. Protein assembly was guided by principles of parsimony to produce the smallest set of proteins necessary to account for all observed peptides (algorithm described in (14)). Where all PSMs from a given HCMV protein could be explained either by a canonical gene or non-canonical ORF, the canonical gene was picked in preference. In a small number of cases, PSMs assigned to a non-canonical or 6FT-ORF were a mixture of peptides from the canonical protein and the ORF. This most commonly occurred where the ORF was a 5'-terminal extension of the canonical protein (thus meaning that the smallest set of proteins necessary to account for all observed peptides included the ORFs alone). In these cases, the peptides corresponding to the canonical protein were separated from those unique to the ORF, generating two separate entries. In a single case, PSM were assigned to the 6FT-ORF 6FT_6_ORF1202_676aa, which is a 5'-terminal extension of the non-canonical ORF ORFL147C. The principles described above were used to separate these two ORFs. Proteins were quantified by summing TMT reporter ion counts across all matching peptide-spectral matches using ''MassPike'', as described previously (10). Briefly, a 0.003 Th window around the theoretical m/z of each reporter ion was scanned for ions and the maximum intensity nearest to the theoretical m/z was used. The primary determinant of quantitation quality is the number of TMT reporter ions detected in each MS3 spectrum, which is directly proportional to the signal-to-noise (S:N) ratio observed for each ion. Conservatively, every individual peptide used for quantitation was required to contribute sufficient TMT reporter ions so that each on its own could be expected to provide a representative picture of relative protein abundance (10). An isolation specificity filter with a cut-off of 50% was additionally employed to minimise peptide co-isolation (10). Peptide-spectral matches with poor quality MS3 spectra (a combined S:N ratio of less than 120 (**Experiment 1**) or 240 (**Experiment 2**) across all TMT reporter ions) or no MS3 spectra at all were excluded from quantitation. Peptides meeting the stated criteria for reliable quantitation were then summed by parent protein, in effect weighting the contributions of individual peptides to the total protein signal based on their individual TMT reporter ion yields. Protein quantitation values were exported for further analysis in Excel. For protein quantitation, reverse and contaminant proteins were removed, then each reporter ion channel was summed across all quantified proteins and normalised assuming

equal protein loading across all channels. To combine data from 48 h experiments 1 and 2, fractional TMT signals compared to the sum across all three assessed conditions were used. For example, for protein PCDHGB5, three fractions were calculated for each experiment: mock/(sum(mock,HCMV,HCMV+MG)), HCMV/(sum(mock,HCMV,HCMV+MG)), HCMV+MG/(sum(mock,HCMV,HCMV+MG)). Replicate fractions from each experiment were averaged for display in figures, and for the purposes of fold change calculation. This effectively corrected for differences in the numbers of peptides observed per protein. For the TMT-based experiments, both normalised S:N values and fractional TMT signals are presented in **Dataset S1** ('Data' worksheet). For proteins only quantified in one replicate, the '48 h average' plot in this dataset shows the data from the replicate in which the protein was quantified; otherwise, the average and range of the two fractional TMT signals. Data are similarly displayed in **Figures 2D-E**. Although peptides were assigned appropriately to HLA-A alleles, it was not possible to assign peptides confidently to only two HLA-B or HLA-C alleles, and signal:noise values were further summed for each of these alleles to give a single combined result for HLA-B or HLA-C.

Figure 2 and S1B. K-means clustering was performed using Cluster 3.0 (Stanford University) and visualised using Java Treeview (http://jtreeview.sourceforge.net).

Figure S5. Alignment of pUL36 amino acid sequences with performed using Clustal Omega (15) (https://www.ebi.ac.uk/Tools/msa/clustalo/) by EMBL-EBI.

Statistical analysis

Figures 2, S1A and S4A. The method of Significance B was used to estimate the p-value that the fold downregulation or rescue was significantly different to 1 (16). Values were calculated and corrected for multiple hypothesis testing using the method of Benjamini-Hochberg in Perseus version 1.5.2.20 (16).

Figure 3. P-values for enrichment in immunoprecipitations were estimated using the method of Significance A and corrected for multiple hypothesis testing in Perseus version 1.5.2.20 (16).

Figures 4 and 5. P-values were calculated using a Student's two-sample, two-tailed t-test in R version 3.4.1 (17). A Shapiro-Wilk test was used to determine that the data was normally distributed and therefore valid for analysis by a t-test. Homogeneity of variance was confirmed using a Bartlett's test.

Data and materials availability statement

The mass spectrometry proteomics data have been deposited to the ProteomeXchange Consortium (http://www.proteomexchange.org/) via the PRIDE partner repository (18) with the dataset identifier PXD017279. All materials described in this manuscript, and any further details of protocols employed, can be obtained on request from the corresponding author by email to mpw1001@cam.ac.uk.

Supplementary Information Figures

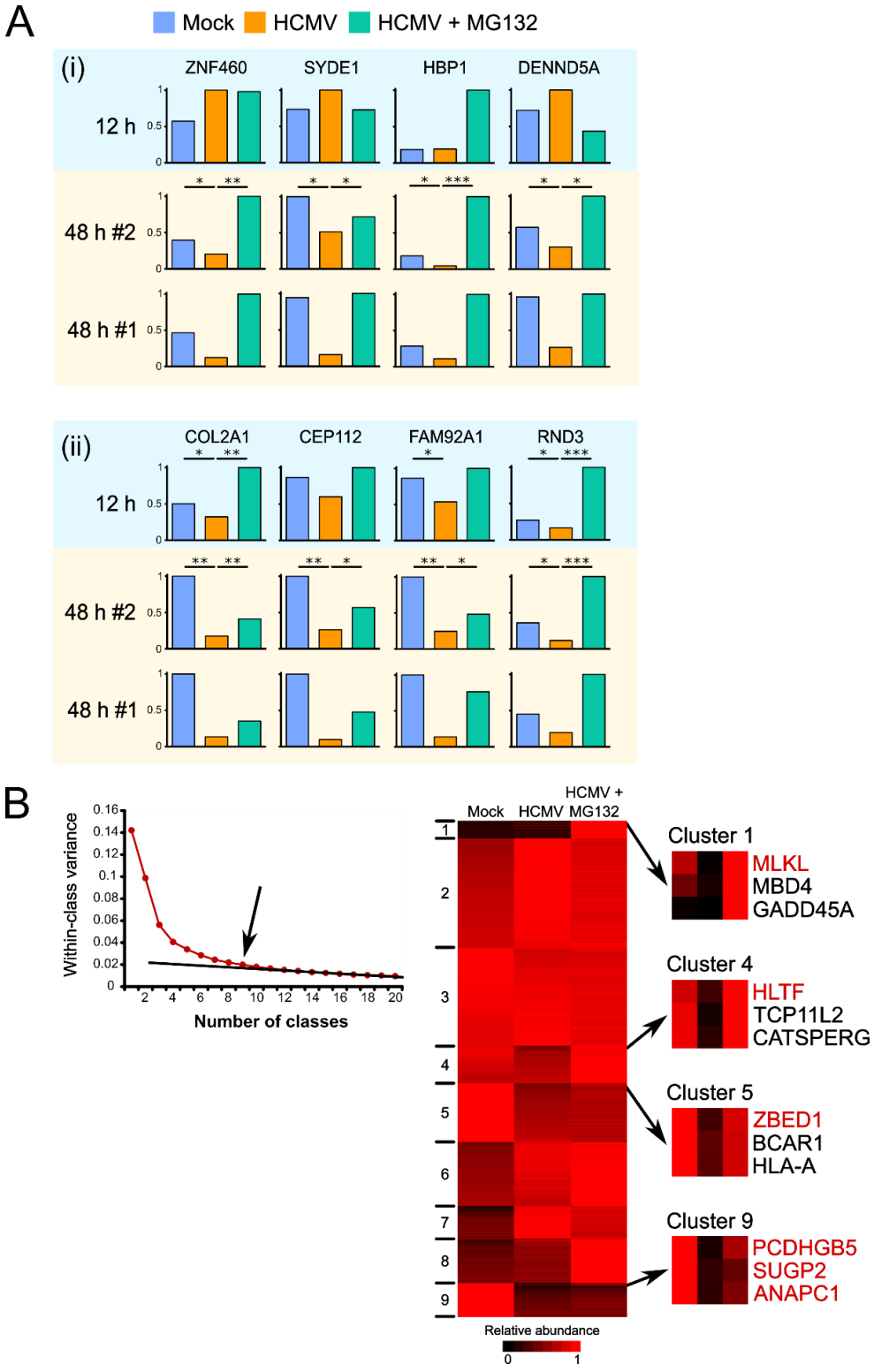

Figure S1. (A) Comparison of 12 and 48 h degradation data for individual proteins. A direct contrast can be made between 12 h data and the second 48 h biological replicate, as both samples were simultaneously digested into peptides, labelled with TMT reagents and analysed. Data for the first 48 h replicate are also shown for comparison. 12 h data were derived by re-analysis of residual protein samples from the Nightingale *et al.* study (5). (i) Four proteins degraded at 48 h but not at 12 h. (ii) Four proteins degraded at 48 h, but insufficiently degraded at 12 h to pass filtering criteria in the Nightingale *et al.* study (5). P-values are shown above the data for 48 h experiment 2 and were derived from ratios generated from averaged data from experiments 1 and 2 using Significance B values **(Figure 2B)** *$p<0.05$, **$p<0.001$, ***$p<1\times10^{-7}$. A full list of proteins degraded late in infection can be found in **Dataset S1**, including details of which are also degraded early. **(B)** K-means-based hierarchical cluster analysis of all human proteins quantified **(Figure 2B)**. K-means clustering with 1-20 classes was used to assess the summed distance of each protein from its cluster centroid. While this summed distance necessarily became smaller as more clusters were added, the rate of decline decreased with each added group, eventually settling at a fairly constant rate of decline that reflected over-fitting; clusters added prior to this point reflected underlying structure in the protein data, while clusters subsequently added through over-fitting were not informative. The point of inflexion fell at or after nine classes, indicating that there were at least nine classes of proteins displaying different expression profiles across the protein samples. The panels on the right show examples of proteins belonging to classes 1, 4, 5 and 9, which contain the 7 proteins degraded early and late during infection **(Figure 2C)**. A full list of proteins in each cluster can be found in **Dataset S1C**.

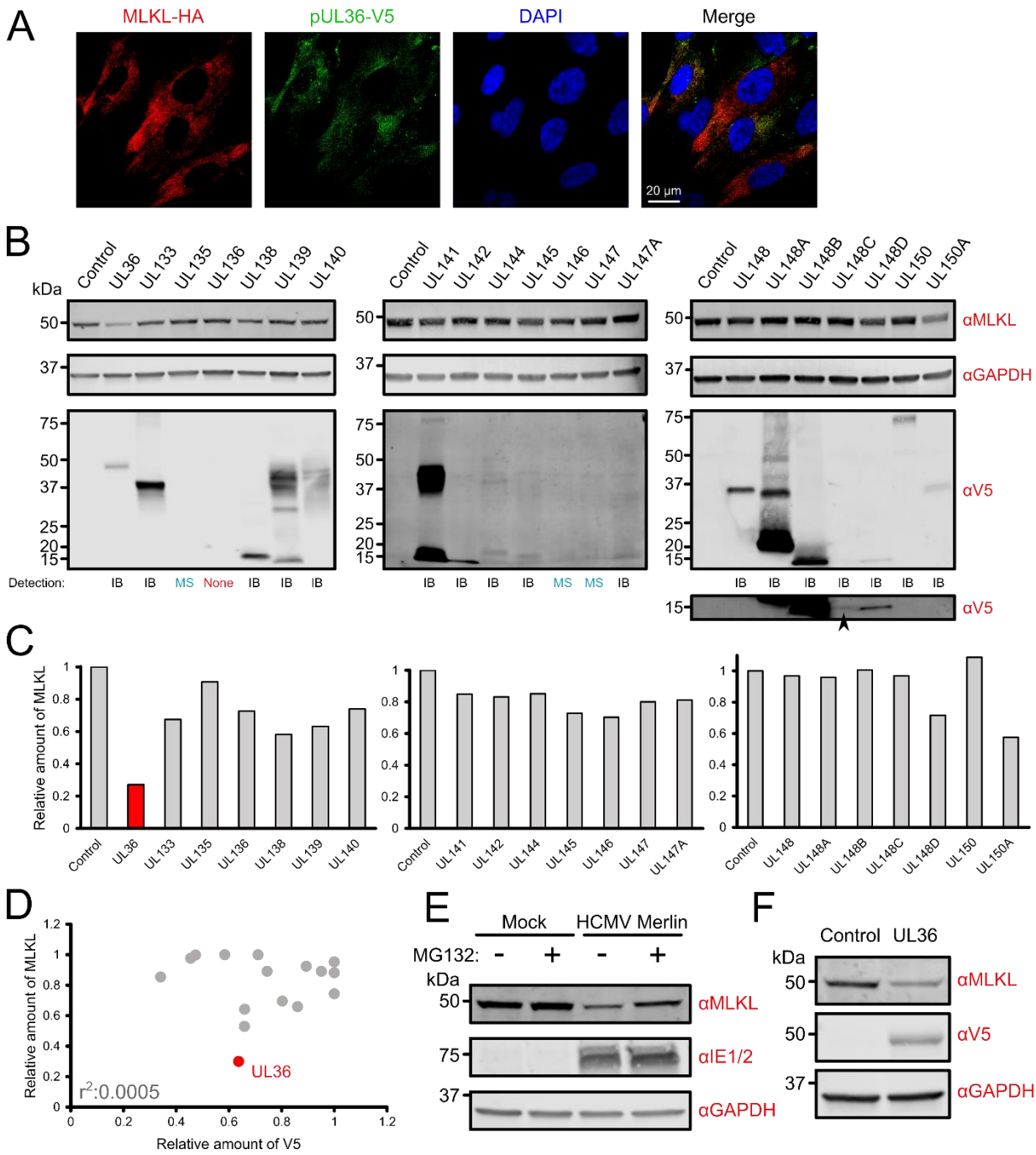
A
MLKL-HA
pUL36-V5
DAPI
Merge
20 μm
B
kDa
Control
UL36
UL133
UL135
UL136
UL138
UL139
UL140
UL141
UL142
UL144
UL145
UL146
UL147
UL147A
UL148
UL148A
UL148B
UL148C
UL148D
UL150
UL150A
αMLKL
αGAPDH
αV5
Detection:
IB
MS
None
C
Relative amount of MLKL
D
Relative amount of MLKL
Relative amount of V5
UL36
r2:0.0005
E
Mock
HCMV Merlin
MG132:
αMLKL
αIE1/2
αGAPDH
F
Control
UL36
αMLKL
αV5
αGAPDH

Figure S2. (A) Immunofluorescence demonstrated diffuse cytoplasmic colocalisation between MLKL-HA and pUL36-V5 in stably co-transduced HFFF-TERTs. **(B)** Immunoblot showing that pUL36 is sufficient to downregulate MLKL. Expression of 17/21 V5-tagged viral proteins was confirmed by anti-V5 immunoblot. Expression of pUL135, pUL146 and pUL147 was confirmed by mass spectrometry (9). pUL136 was not detected by either method; further confirmation that pUL136 does not affect MLKL levels is required, although this protein was not detected in the SILAC IP of MLKL-HA in HCMV-infected cells (**Figure 3C**). A faint band corresponding to pUL148C could be detected upon over-exposure of the blot (bottom right panel). **(C)** Densitometry analysis of MLKL expression normalised by GAPDH expression in each cell line. Expression of UL36 was sufficient to reduce the level of MLKL by 3.7-fold. MLKL expression was not modulated more than 2-fold by other proteins in the UL/b' region. **(D)** Despite substantial variation in the level of expression of some of the viral proteins, this did not correlate with relative MLKL abundance. For every cell line in which V5 was detectable by immunoblotting, the relative abundances of MLKL (adjusted to GAPDH) and the V5-tagged viral protein (adjusted to GAPDH) were calculated. To prevent confounding effects from systematic expression level differences between each of the three blots, values derived from each blot were normalised to the maximum level of MLKL and V5 expression prior to comparison. No correlation between MLKL and V5 expression was observed. **(E)** Immunoblot confirming that MLKL is degraded by HCMV strain Merlin in cells solubilised in 2% SDS as well as in cells lysed in RIPA buffer **(Figure 3B)**. The level of MLKL was partially recovered by addition of MG132, indicating active degradation (MOI = 5, 48 h infection). MG132 at a final concentration of 10 μM or an equivalent volume of DMSO was added to media for the last 12 h of infection. **(F)** Immunoblot confirming that MLKL is downregulated by pUL36 in cells solubilised in 2% SDS as well as in cells lysed in RIPA buffer **(Figure 3E)**.

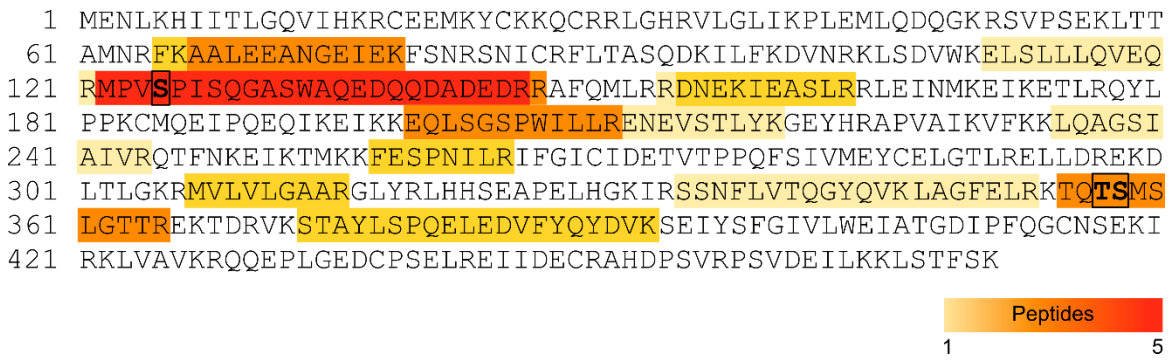

Figure S3. pUL36 interacts with unphosphorylated MLKL. Amino acid sequence of MLKL, with the peptides identified in the pUL36-V5 IP **(Figure 3D)** highlighted in different colours according to the frequency of identification. Thr357 and Ser358 are phosphorylated by RIP3 during TNFα-stimulated necroptosis (19). Ser125 is phosphorylated in a cell-cycle dependent manner but its effect on MLKL function is unknown (20, 21). No phospho-MLKL peptides were identified.

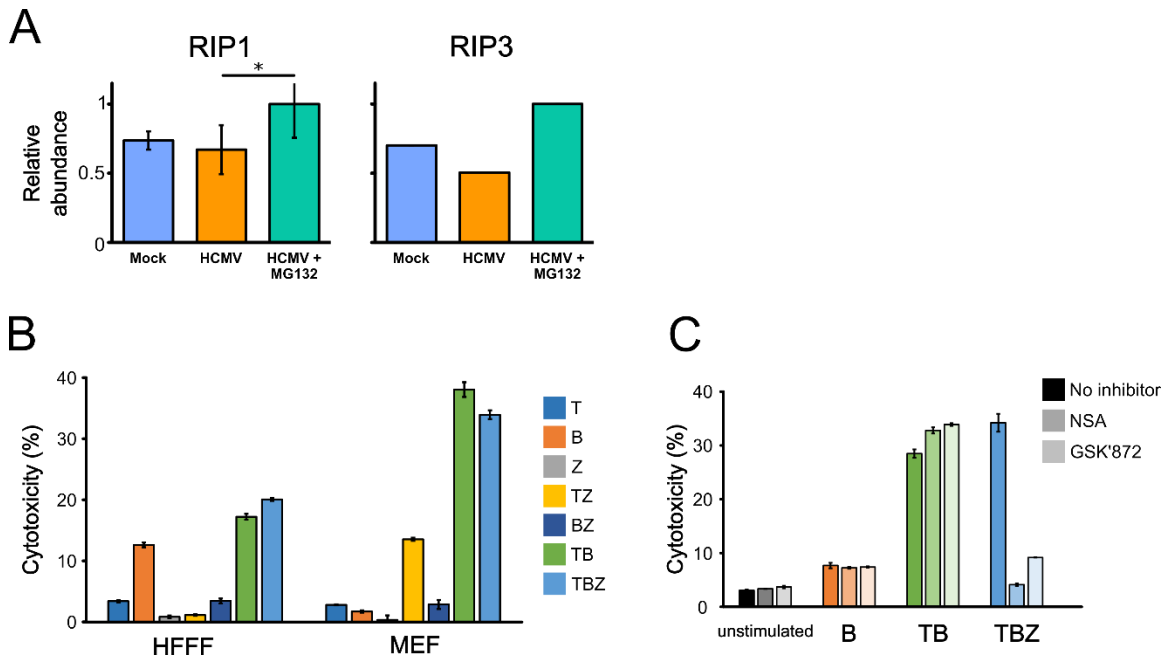

Figure S4. **(A)** Expression of RIP1 and RIP3 in HFFF-TERTs quantified by proteomics (the experimental setup is described in **Figure 2**). RIP3 was only detected in the first of two biological replicates. *p<0.05. **(B)** Cell death in HFFF-TERTs is stimulated by BV6 (B) alone, TNFα + BV6 (TB), and TNFα + BV6 + Z-VAD-fmk (TBZ). In addition to apoptosis stimulated by TB and necroptosis stimulated by TBZ, HFFFs also underwent cell death in response to B alone, which has been described in other cell types (22). Cell death in MEFs was additionally stimulated by TZ, which has been observed in other mouse fibroblast cell lines (23). Each treatment was applied for 18 h. Error bars show standard error of the mean (SEM). Data are representative of three independent experiments. **(C)** Cell death in HFFF-TERTs stimulated by TBZ is RIP3- and MLKL-dependent, whereas B or TB stimulate pathways independent of RIP3 and MLKL. Cells were treated for 18 h in the presence or absence of necrosulfonamide (NSA) or GSK'872. Application of NSA and GSK'872 in the absence of T, B or Z indicated that the inhibitors did not impact cell viability.

```
 AD169  MDDLRDTLMAYGCIAIRAGDFNGLNDFLEQECGTRLHVAWPERCFIQLRSRSALGPFVGK  60
Merlin  MDDLRDTLMAYGCIAIRAGDFNGLNDFLEQECGTRLHVAWPERCFIQLRSRSALGPFVGK  60
        ************************************************************

 AD169  MGTVCSQGAYVCCQEYLHPFGFVEGPGFMRYQLIVLIGQRGGIYCYDDLRDCVYELAPTM  120
Merlin  MGTVCSQGAYVCCQEYLHPFGFVEGPGFMRYQLIVLIGQRGGIYCYDDLRDCIYELAPTM  120
        ************************************************:*******

 AD169  KDFLRNGFRHRDHFHTMRDYQRPMVQYDDYWNAVMLYRGDVESLSAEVTKRGYASYTIDD  180
Merlin  KDFLRHGFRHCDHFHTMRDYQRPMVQYDDYWNAVMLYRGDVESLSAEVTKRGYASYSIDD  180
        *****:**** ************************************************:***

 AD169  PFDECPDTHFAFWTHNTEVMKFKETSFSVVRAGGSIQTMELMIRTVPRITCYHQLLGALG  240
Merlin  PFDECPDTHFAFWTHNTEVMKFKETSFSVVRAGGSIQTMELMIRTVPRITCYHQLLGALG  240
        ************************************************************

 AD169  HEVPERKEFLVRQYVLVDTFGVVYGYDPAMDAVYRLAEDVVMFTCVMGKKGHRNHRFSGR  300
Merlin  HEVPERKEFLVRQYVLVDTFGVVYGYDPAMDAVYRLAEDVVMFTCVMGKKGHRNHRFSGR  300
        ************************************************************

 AD169  REAIVRLEKTPTCQHPKKTPDPMIMFDEDDDDELSLPRNVMTHEEAESRLYDAITENLMH  360
Merlin  REAIVRLEKTPTCQHPKKTPDPMIMFDEDDDDELSLPRNVMTHEEAESRLYDAITENLMH  360
        ************************************************************

 AD169  CVKLVTTDSPLATHLWPQELQALCDSPALSLCTDDVEGVRQKLRARTGSLHHFELSYRFH  420
Merlin  CVKLVTTDSPLATHLWPQELQALCDSPALSLCTDDVEGVRQKLRARTGSLHHFELSYRFH  420
        ************************************************************

 AD169  DEDPETYMGFLWDIPSCDRCVRRRRFKVCDVGRRHIIPGAANGMPPLTPPHVYMNN     476
Merlin  DEDPETYMGFLWDIPSCDRCVRRRRFKVCDVGRRHIIPGAANGMPPLTPPHAYMNN
        ************************************************.****
```

Figure S5. Amino acid sequence alignment of pUL36 from HCMV strains Merlin and AD169 using Clustal Omega by EMBL-EBI (15). The five amino acid sequence differences are highlighted. '*' indicates positions which have an identical, fully conserved residue. ':' indicates a substitution with a residue with strongly similar properties. '.' indicates a substitution with a residue with weakly similar properties.

Supplementary Information Legends for Datasets

Dataset S1 (separate .xls file). Interactive spreadsheet of all TMT-based proteomic data in this paper. The 'Plotter' worksheet generates graphs of protein abundance for any human or viral protein quantified across each experiment. The 'Data' worksheet shows minimally annotated protein data, for which the only modifications are formatting, deletion of contaminants, normalisation and reassignment of non-canonical HCMV ORFs. The 'K-means clusters' worksheet shows the human proteins belonging to each cluster from **Figure S1B**.

Dataset S2 (separate .xls file). Data from the MLKL-HA (denoted 'HA') and pUL36-V5 (denoted 'V5') SILAC immunoprecipitations.

Dataset S3 (separate .xls file). (A) Oligonucleotides employed in PCR amplification of MLKL-HA and the V5-tagged viral genes used in the study. **(B)** Confirmed sequences of MLKL-HA and the viral genes UL36 and UL133-150A. **(C)** Oligonucleotides employed for site-directed mutagenesis of UL36. **(D)** Method of cloning and verification of expression of each of the viral genes UL36 and UL133-150A.

Supplementary Information References

1. McSharry BP, Jones CJ, Skinner JW, Kipling D, Wilkinson GWG (2001) Human telomerase reverse transcriptase-immortalized MRC-5 and HCA2 human fibroblasts are fully permissive for human cytomegalovirus. *J Gen Virol* 82:855–863.
2. Allison R, et al. (2017) Defects in ER-endosome contacts impact lysosome function in hereditary spastic paraplegia. *J Cell Biol* 216(5):1337–1355.
3. Dolan A, et al. (2004) Genetic content of wild-type human cytomegalovirus. *J Gen Virol* 85(5):1301–1312.
4. Stanton RJ, et al. (2010) Reconstruction of the complete human cytomegalovirus genome in a BAC reveals RL13 to be a potent inhibitor of replication. *J Clin Invest* 120(9).
5. Nightingale K, et al. (2018) High-definition analysis of host protein stability during human cytomegalovirus infection reveals antiviral factors and viral evasion mechanisms. *Cell Host Microbe* 24:1–14.
6. Stanton RJ, et al. (2007) Cytomegalovirus destruction of focal adhesions revealed in a high-throughput Western blot analysis of cellular protein expression. *J Virol* 81(15):7860–72.
7. Fielding CA, et al. (2014) Two novel human cytomegalovirus NK cell evasion functions target MICA for lysosomal degradation. *PLoS Pathog* 10(5).

8. Tanaka J, et al. (1984) Enhanced Replication of Human Cytomegalovirus in Human Fibroblasts Treated with Dexamethasone. *J gen Virol* 65:1759–1767.

9. Nobre L V, et al. (2019) Human cytomegalovirus interactome analysis identifies degradation hubs, domain associations and viral protein functions. *Elife* 8(e49894).

10. McAlister GC, et al. (2014) MultiNotch MS3 enables accurate, sensitive, and multiplexed detection of differential expression across cancer cell line proteomes. *Anal Chem* 86(14):7150–7158.

11. McAlister GC, et al. (2012) Increasing the multiplexing capacity of TMT using reporter ion isotopologues with isobaric masses. *Anal Chem* 84:7469–7478.

12. Hartley JL, Temple GF, Brasch MA (2000) DNA cloning using in vitro site-specific recombination. *Genome Res* 10:1788–1795.

13. Stern-Ginossar N, et al. (2012) Decoding human cytomegalovirus. *Science (80-)* 338(6110).

14. Huttlin EL, et al. (2010) A tissue-specific atlas of mouse protein phosphorylation and expression. *Cell* 143(7):1174–1189.

15. Sievers F, et al. (2011) Fast, scalable generation of high-quality protein multiple sequence alignments using Clustal Omega. *Mol Syst Biol* 7(1):539.

16. Cox J, Mann M (2008) MaxQuant enables high peptide identification rates, individualized p.p.b.-range mass accuracies and proteome-wide protein quantification. *Nat Biotechnol* 26(12):1367–1372.

17. R Core Team (2018) R: A language and environment for statistical computing. Available at: https://www.r-project.org/.

18. Vizcaíno JA, et al. (2016) 2016 update of the PRIDE database and its related tools. *Nucleic Acids Res* 44(D1):D447–D456.

19. Wang H, et al. (2014) Mixed lineage kinase domain-like protein MLKL causes necrotic membrane disruption upon phosphorylation by RIP3. *Mol Cell* 54(1):133–146.

20. Dephoure N, et al. (2008) A quantitative atlas of mitotic phosphorylation. *PNAS* 105(31):10762–10767.

21. Daub H, et al. (2008) Kinase-selective enrichment enables quantitative phosphoproteomics of the kinome across the cell cycle. *Mol Cell* 31(3):438–448.

22. Christofferson DE, Li Y, Yuan J (2014) Control of life-or-death decisions by RIP1 kinase. *Annu Rev Physiol* 76(1):129–150.

23. Ros U, et al. (2017) Necroptosis execution is mediated by plasma membrane nanopores independent of calcium. *Cell Rep* 19(1):175–187.